A Novel Efficient Method for Total Transfer Capability Evaluation of a Power System Integrated with Renewable Energy

再生可能エネルギーを大量導入した電力系統における効率的な送電可能容量算出手法に関する研究

パンスワン　ナッタウット

A dissertation submitted in partial fulfillment of the requirements
of the degree of Doctor of Philosophy in the
Graduate School of Engineering, The University of Tokyo

December 2010

Acknowledgements

First of all I would like to express my sincere gratitude and appreciation to my advisor, Professor Akihiko Yokoyama for his kind and continuous guidance, invaluable support and encouragement throughout my study. It has been a very great pleasure to me to conduct this research under his supervision.

Besides, I am grateful to Professor Kunihiko Hidaka, Professor Haruhito Taniguchi, Professor Takafumi Koseki, Professor Hiroyuki Ohsaki, and Professor Jumpei Baba, the committee of my Ph.D. dissertation. Without their comments and suggestions, this research definitely cannot be completed.

I would also like to thank Mr. Norihito Shimada sincerely for his kind assistance and various technical supports during my stay in Yokoyama laboratory. Special thanks are due to Dr. Surachai Chaitusaney, Dr. Jun Zhang, and Dr. Kritsana Tangpatiphan who are my respectful seniors for their kind help and guidance in both academic and Japanese language matters. Also, special thanks to Mr. Ko Sekita as my tutor for his kind assistance since my first days in Japan. In addition to the people mentioned above, other members and past members are also highly appreciated for the accomplishment of my doctoral degree. They are Mr. Shinji Ooya, Mr. Ken-ichi Kawabe, Mr. Hiroshi Irie, Mr. Taisuke Masuta, Mr. Nguyen Hoang Viet and so on. I particularly thank Mr. Hiroshi Irie and Mr. Ken-ichi Kawabe for their contribution towards making our lab a big family.

Special thanks go to Dr. Suresh Chand Verma, and Dr. Nakachi Yoshiki from Chubu Electric Power Co., Inc. for their collaboration in this research work.

I am indebted to all staff members of the office of Department of Electrical Engineering, Graduate School of Engineering who have directly and indirectly supported me during my study.

Thanks to the Ministry of Education, Culture, Sports, Science and Technology of Japan for providing me the scholarship and giving me the chance to study at the University of Tokyo.

Finally, I am deeply grateful to my beloved parents and sister for their love, understanding, continuous encouragement, and support.

Paensuwan Nattawut
Tokyo
December 2010

List of Figures

List of Tables

Contents

Chapter 1

Introduction

1.1 Background

Managing the security of a transmission network has always been one of the challenging tasks for system operators, particularly within a deregulated environment where the transmission network is usually operated close to its limits, and congestion problems are common. Consequently, this provokes utilities to evaluate the transfer capability as an index measuring the ability of the transmission network to carry or move electric power from one location to another across the system. Indeed, this index provides the system operators beforehand with useful information regarding one of the operational limits of the transmission network, helping them manage the energy trading or transmission network security more efficiently.

The transfer capability concept was originally introduced by North American Electric Reliability Council (NERC) in 1995 [1], publishing a report which defines the term 'capability' and distinguishes it from a closely related term 'capacity.' The terms 'Transfer capability' and 'Transmission capacity' are different. In transmission systems, the term 'capacity' commonly refers to the thermal limit or rating of a particular transmission component, e.g. a transmission line or transformer. On the other hand, the term 'capability' refers to the ability, i.e. the amount of the capacity which can be utilized while satisfying a set of specified conditions. Based on this terminology, the transfer capability was defined as a measure of the ability of an electric system to reliably move or transfer electric power from one location to another over all transmission lines (or paths) between those locations under specified system conditions. In this context, 'location' may be individual electric power system, power pool, control area, sub-region, or portion of any of these. Later in 1996, NERC released another document on Available Transfer Capability (ATC), introducing several new additional terms, e.g. transmission margins to account for the uncertainty and system reliability, and Total Transfer Capability (TTC).

Several important aspects should be taken into consideration when evaluating the transfer capability, e.g. uncertainty associated with the system operating conditions and parameters, and security constraints related to voltage and transient stabilities. Uncertainty has always been with the operation and planning of a power system. It has been realized essential by power industries, particularly in the near future power system where a large penetration of renewable energy is expected. As is known, unlike conventional energy sources, renewable energy

sources have very limited dispatchability and their power output is uncertain and strongly fluctuating with the wind speed or climate. In addition to the uncertainty, security requirements are of primary concern for a secure operation of a power system where several constraints, i.e. voltage and transient stabilities, should be properly taken into consideration. Voltage stability is needed to be ensured such that the system is operated with a sufficient margin away from the voltage collapse point. Transient stability is also an important aspect so as to ensure synchronism under contingency circumstances following large disturbances. These requirements simply impose technical challenges to the transfer capability evaluation. Incorporating all of them into the evaluation is computationally intensive and complex due mainly to the non-linear nature of a power system. Therefore, it is necessary to develop a comprehensive scheme for the transfer capability evaluation where all requirements are fully addressed, and also effective techniques to improve the computational speed.

1.2 Review of TTC and Evaluation Methods

Total Transfer Capability (TTC) is an index which measures the ability of a transmission network to carry or move electric power from one location to another across the system. It also represents one of the system operational limits, useful information and guideline for the system operators in managing the security of a transmission network, especially under a competitive environment where the transmission network is usually operated close to its limit, and congestion problems are common. The TTC was defined by NERC in its document released in 1996 as part of the Available Transfer Capability (ATC) determination. Mathematically, ATC is expressed as a function of several related terms as shown in the following equation. Their relationship is depicted in Figure 1.

$$ATC = TTC - TRM - CBM - ETC. \tag{1.1}$$

The definition of each term in Eq. (1.1) is given as follows [2]:

Available Transfer Capability (ATC) is a measure of the transfer capability remaining in the physical transmission network for further commercial activity over its committed use without jeopardizing the power system security.

Total Transfer Capability (TTC) is the maximum of power that can be transferred in a reliable manner between a pair of defined source and sink locations in the interconnected system while meeting all of a specific set of defined pre- and post- contingency system conditions.

Transmission Reliability Margin (TRM) is the amount of transfer capability necessary to provide a reasonable level of assurance that the interconnected transmission network will be secure. In other words, TRM is a reserved margin that accounts for inherent uncertainty in system conditions to ensure the flexible and reliable operation as system conditions change.

Capacity Benefit Margin (CBM) is the amount of transfer capability preserved for Load Service Entities (LSE's) on the host transmission system where their load is located, to enable an access to generation from interconnected systems to meet generation reliability requirements.

Existing Transfer Commitment (ETC) is the amount of electric power which has been already committed or scheduled, i.e. base-case electric power transfer.

The physical interpretation of each term is given in the following. Given a transmission network, usually some portion of the capacity is already committed as the base-case transfer projecting into the future, e.g. a day ahead. This portion of the scheduled electric power is referred as the ETC. Above this already committed use, only portion of the total transmission capacity can be utilized reliably and safely in transferring additional electric power. Consequently, the total amount of reliably and securely transferable electric power is denoted as TTC. In addition, as the power industries have gained experience over the years, it is found that some transmission margins should be preserved to account for the uncertainty associated with the system conditions and for achieving the system reliability level. As a result, two additional transmission margins were introduced, i.e. TRM and CBM respectively. TRM is a

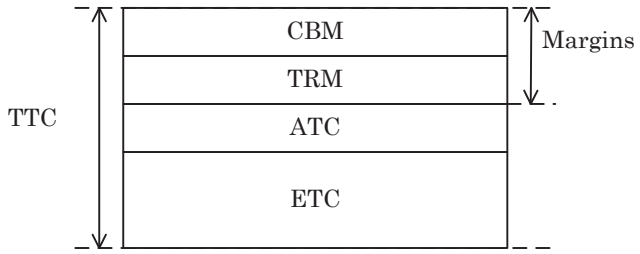

Figure 1: Relationship among ATC, TTC, TRM, CBM, and ETC.

margin to be preserved to account for the impact of the uncertainty which is mainly attributed to the outages on transmission facilities, the error of forecast parameters, e.g. demand and power output from renewable energy sources. This margin will give a level of assurance of the system security and reliability under a system condition change. The other margin, CBM is preserved mainly for the reliability purpose. In case of an interconnected power system, this margin is intended to be used only in times of emergency generation deficiency of any of the systems within the interconnected system. In other words, the system with insufficient generation can receive the assist from its neighboring systems through this preserved margin to meet its demand. Hence, this preservation of CBM can help improve the overall system reliability.

Total Transfer Capability (TTC) is the most important and the first term to be determined in the ATC determination. The TTC evaluation is commonly based on computer simulations of the operation of a system under a specific set of assumed operating conditions. These simulations are usually performed offline in advance, e.g. a day ahead. Up to present, there have been several methods proposed for the TTC evaluation. In general, they can be classified into deterministic and probabilistic approaches. The deterministic approach evaluates the transfer capability for a given set of system conditions, e.g. all N-1 contingencies, and the minimum is set as the TTC [3], [4]. This approach is simple but rather conservative which may lead to ineffective use of the transmission network. The farther into the future that the simulations are projected, the greater the uncertainty. With this regard, the probabilistic methods seem to be more appropriate due mainly to their ability to recognize and cope with the uncertainty. A number of literatures on the TTC evaluation by means of the probabilistic approaches have been well reported. In [5], the TTC is evaluated using stochastic programming. In [6], R.F. Chang *et. al.* employ bootstrap technique to find the TTC. In addition, the TTC can be evaluated by means of Monte Carlo simulation [7]–[9]. Although the probabilistic approach is with high computational cost, it is preferable over the deterministic counterpart. Furthermore, the presence of renewable energy, e.g. wind power and photovoltaic (PV), emphasizes the use of the probabilistic approach.

Regardless the approaches used, the main calculation in the TTC evaluation is to compute the maximum transferable power for a given system operating condition. This maximum transferable power is often referred as Maximum Transfer Capability (MTC) in a number of TTC literatures. Several methods for the MTC calculation are listed below with the detailed descriptions summarized in the following subsections.

1. Repeated power flow (RPF) [10]
2. Continuation power flow (CPF) [11], [12]
3. Two-step method [13]
4. Optimal power flow (OPF) [14]

1.2.1 Repeated Power Flow (RPF)

Repeated Power Flow (RPF), as the name implies, finds the MTC by successively solving a set of power flow problems. The demand at the sink, and generation at the source are increased in an increment step until any of the following constraints are violated.

1. Voltage magnitude limit: System voltage magnitude must be maintained within the range of acceptable minimum and maximum limits.
2. Thermal limit: Thermal limit establishes the maximum amount of electrical current that a transmission line or electrical facility can conduct over the specified time period before it sustains permanent damage by overheating.
3. Generation capacity limit: Generation at the source should not exceed its active power and reactive power capacity limits.

Note that this method is based on power flow calculation; as a result, the security constraints related to transient stability is not considered. Although RPF is time-consuming due to the repetition of the power flow calculation, its algorithm is simple and without much computational requirement.

1.2.2 Continuation Power Flow (CPF)

Continuation Power Flow (CPF) was originally introduced to determine maximum loadability for voltage stability study [12]. Nonetheless, the principle behind the CPF is found applicable for other applications including the MTC calculation. Similar to RPF, the CPF algorithm successively solves the power flow problem. In each step, the control parameters are increased in an increment step, i.e. demand at the sink and generation at the source. The procedure is repeated until the nose-point is reached. Instead of directly successively solving a set of power flow equations, CPF solves a set of augmented power flow equations to trace the trajectory of

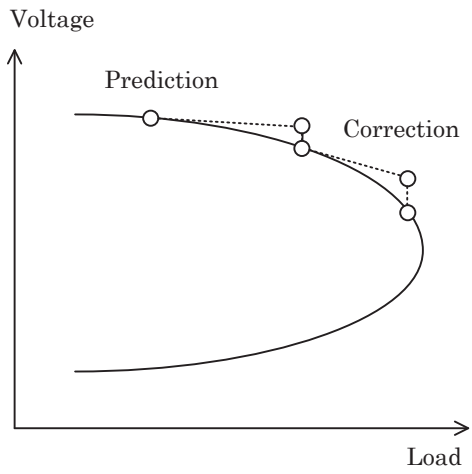

Figure 2: Trajectory of the solution of CPF.

the solution curve passing through the nose-point without encountering numerical difficulty of ill-conditioning as depicted in Figure 2.

As seen from Figure 2, the algorithm of CPF has two main steps; prediction step (Predictor) and correction step (Corrector) respectively. The prediction step predicts the next system operating point after increasing the transfer along the tangent direction. The correction step then moves the predicted operating point to an actual one on the nose curve. The algorithm of CPF is summarized as follows:

Prediction step: The power flow equations are reformulated. The net active and reactive power injections at the sink and source buses are modified to include λ which represents the direction of the load increase.

$$P_i = P_i^0 + \lambda K_i \tag{1.2}$$

$$Q_i = Q_i^0 + \lambda K_i \tag{1.3}$$

Here P_i^0 ,Q_i^0 are base-case active and reactive power at bus i, and K_i is a factor specifying the rate of change of the load at bus i. The modified power flow equations can be expressed in a compact form as

$$f(\delta, V, \lambda) = 0. \tag{1.4}$$

Here δ is a vector of bus voltage angle, and V is a vector of bus voltage magnitude respectively. The prediction step predicts the next operating point by taking an appropriate step size along the tangent direction which is computed from $t = [d\delta, dV, d\lambda]^T$

$$\begin{bmatrix} f_\delta & f_V & f_\lambda \\ & e_k & \end{bmatrix} \begin{bmatrix} t \end{bmatrix} = \begin{bmatrix} 0 \\ \pm 1 \end{bmatrix} \tag{1.5}$$

where e_k is a zero row vector except the kth element which is 1, and f_δ, f_V, f_λ are computed from

$$d\left[f(\delta, V, \lambda)\right] = f_\delta d\delta + f_V dV + f_\lambda d\lambda. \tag{1.6}$$

Since Eq. (1.6) is rank deficient, an arbitrary value such as 1 is assigned to the kth element of the tangent vector. With the corresponding e_k, Eq. (1.5) can be solved. Whether +1 or -1 is used depends on how the kth element is changing as the solution path is being traced. The kth element is called a *continuation parameter*. The question is that which system state variable should be selected as the continuation parameter. The answer is based on the principle that a continuation parameter should correspond to the system state variable which possesses the largest tangent vector component. For instance, given a normal loading power system, the scalar λ is probably the best candidate when starting from the base-case solution, since, under such conditions, the load change has only slight impact on both voltage magnitudes and angles which fairly remain constant. On the other hand, after the load has been increased for several steps, the solution path is moving close to the critical point where both voltage magnitudes and angles can possibly experience a significant change. Therefore, it is selected from the largest element of the tangent vector, i.e.

$$x_k = \max\left\{t_1, t_2, ..., t_m\right\}. \tag{1.7}$$

The predicted operating point will then be computed from

$$\begin{bmatrix} \delta^* \\ V^* \\ \lambda^* \end{bmatrix} = \begin{bmatrix} \delta \\ V \\ \lambda \end{bmatrix} + \alpha \begin{bmatrix} d\delta \\ dV \\ d\lambda \end{bmatrix}. \tag{1.8}$$

Here α is a step size.

Correction step: This step corrects the predicted solution obtained in previous step by expanding on parameterization. In other words, the corrector is an augmented power flow in which the Jacobian matrix is augmented by an equation accounting for the continuation parameter. Let $x = [\delta, V, \lambda]^T$ and $x_k = \eta$; the augmented power flow can be written as

$$\begin{bmatrix} f(x) \\ x_k - \eta \end{bmatrix} = [0]. \tag{1.9}$$

This augmented power flow problem can also be solved by Newton Raphson's method. Once the nose curve is determined, the corresponding MTC can be found.

1.2.3 Two-Step Method

Two-Step method was proposed in [13]. This method has prediction and correction steps. The prediction step makes use of the first-order sensitivities to predict the active constraint which limits the transfer. The correction step then augments the predicted active constraint

into the power flow equations. For each MTC calculation, this method takes only two steps; thus, resulting in short computation time when compared with CPF which may take several successive steps. Both steps are discussed in detail in the following.

Prediction step: Prediction of the active constraint is based on the sensitivity index, SI calculated from the sensitivities related to the system constraints, e.g. voltage magnitude limit, transmission line thermal limit, generation capacity limit, with respect to the increment of demand at the sink bus which is denoted by a scalar λ. By comparing the sensitivity indices related to each constraint, the index with the highest value is selected as a predicted active constraint. The sensitivity indices related to voltage magnitude limit, SI_V, transmission line thermal limit, SI_S, generation capacity limit, SI_{P_G} are computed from

$$SI_V = \frac{dV_i/d\lambda}{\Delta V_{i,tol}} \tag{1.10}$$

$$SI_S = \frac{dS_{ij}/d\lambda}{\Delta S_{ij,tol}} \tag{1.11}$$

$$SI_{P_G} = \frac{dP_G/d\lambda}{\Delta P_{G,tol}} \tag{1.12}$$

where $V_i, \Delta V_{i,tol}$ are the voltage magnitude of bus i and its maximum tolerance; $S_{ij}, \Delta S_{ij,tol}$ are the apparent power flow from bus i to bus j and its maximum tolerance; $P_G, \Delta P_G$ are the active power generation at the source and its maximum tolerance.

Correction step: Similar to the correction scheme in CPF, the correction step of the two-step method is based on the parameterization. Solving for the system state variables including a scalar λ requires another equation which is the predicted active constraint obtained in the prediction step. The modified power balance equations are the same as for CPF and the predicted active constraint which is a function of system state variables, $f(\delta, V, \lambda) = f_{limit}$. Consequently, the Jacobian matrix is modified as follows

$$\begin{bmatrix} \frac{\partial f_P}{\partial \delta} & \frac{\partial f_P}{\partial V} & \frac{\partial f_P}{\partial \lambda} \\ \frac{\partial f_Q}{\partial \delta} & \frac{\partial f_Q}{\partial V} & \frac{\partial f_Q}{\partial \lambda} \\ \frac{\partial f_{limit}}{\partial \delta} & \frac{\partial f_{limit}}{\partial V} & \frac{\partial f_{limit}}{\partial \lambda} \end{bmatrix} \begin{bmatrix} \Delta\delta \\ \Delta V \\ \Delta s \end{bmatrix} = \begin{bmatrix} \Delta f_P \\ \Delta f_Q \\ \Delta f_{limit} \end{bmatrix}. \tag{1.13}$$

The augmented row vector corresponding to the predicted active constraint is calculated based on the type of the limiting constraints. Once the power flow is solved, the MTC can be computed directly from the obtained λ. Nonetheless, it is possible that the obtained solution may result in more than one constraint violations. In such cases, the transfer volume is reduced and then the system constraints are rechecked.

1.2.4 Optimal Power Flow (OPF)

MTC can also be determined by solving the optimization problem in which the power transfer is maximized. The details of the formulation of OPF problem will be explained. Although

OPF may consume longer computation time, it gives an accurate and non-conservative result when compared to that obtained from power flow based methods.

The optimization problem is formulated by first introducing a scalar, λ representing a load parameter. As a result, the active and reactive demands at sink buses are modified as follows:

$$P_D = P_D^0 + \lambda \cos(\psi^0) \tag{1.14}$$

$$Q_D = Q_D^0 + \lambda \sin(\psi^0) \tag{1.15}$$

where P_D, Q_D are active and reactive loads at the sink bus; P_D^0, Q_D^0 are base-case active and reactive loads at the sink bus; ψ^0 is the base-case power factor angle of the sink bus.

This problem can be formulated as an OPF problem with the objective function to maximize the transfer by maximizing λ.

$$\left.\begin{array}{l} \max \quad \lambda \\ \text{s.t.} \\ G(x,\lambda) = 0 \\ H(x,\lambda) \leq 0 \end{array}\right\} \tag{1.16}$$

where x is a vector of system control and state variables, $G(x,\lambda)$ are a set of equality constraints representing the power balance equations, and $H(x,\lambda)$ are a set of inequality constraints representing the system security limits including voltage magnitude limit, generation capacity limit, and equipment thermal limit. Once the maximum λ is successfully solved, the MTC is computed from

$$MTC = P_D^0 + \lambda_{\max} \cos(\psi^0). \tag{1.17}$$

Another technical challenge for the TTC evaluation is the integration of the security constraints related to the voltage and transient stabilities. Voltage stability is usually neglected in the TTC evaluation with the commonly used assumption that the bus voltage magnitude is violated well before the system reaches the voltage collapse point. In some studies [11], Continuation Power Flow (CPF) is used to integrate the voltage stability into the TTC evaluation. Further, in many power systems, the transfer is restricted by the transient stability constraint following large disturbances. Some studies include the transient stability constraint into the TTC evaluation using Transient Stability Constrained Optimal Power Flow (TSCOPF) [15], or energy function methods [16]–[18]. Nonetheless, most of these studies are simply limited to a system with only synchronous generators, and there is currently no investigation on a system integrated with renewable energy.

1.3 Objectives of this Research

The objectives of this research are summarized as follows. The author hopes that this research can help people to have more understanding of one of the power system operational limits, the transfer capability, and its evaluation using a probabilistic method. This research is useful for system planning and operation of the future power system where a large penetration of renewable energy is expected.

1. Review the literatures on the transfer capability and its evaluation using probabilistic methods.
2. Study the transient and voltage stabilities and how to incorporate these issues into the transfer capability evaluation.)
3. Study and develop a model for renewable energy based generation.
4. Develop a methodology based on the probabilistic method to evaluate the transfer capability with voltage and transient stability consideration and check its validity through the numerical simulation.
5. Develop an efficient TTC evaluation method and examine its performance in terms of the accuracy and computational speed enhancement.
6. Review the literatures on LVRT and incorporate it into the TTC evaluation.

1.4 Structure of Dissertation

Chapter 1 mentions the background on the transfer capability evaluated through the TTC index, as well as states both the motivation and objectives of this research. Chapter 2 begins with the algorithm of the proposed TTC evaluation using the Monte Carlo method and describes how to include voltage and transient stability constraints into the evaluation. In the end of the chapter, the framework for the TTC evaluation with Low Voltage Ride-Through (LVRT) consideration is presented. Chapter 3 presents the modeling for two renewable energy based generation technologies, wind power and photovoltaic (PV). Chapter 4 describes the proposed efficient TTC evaluation method using system case partitioning technique and decision tree classification. Numerical examples, results, and discussion are presented in Chapter 5. Finally, Chapter 6 concludes the dissertation.

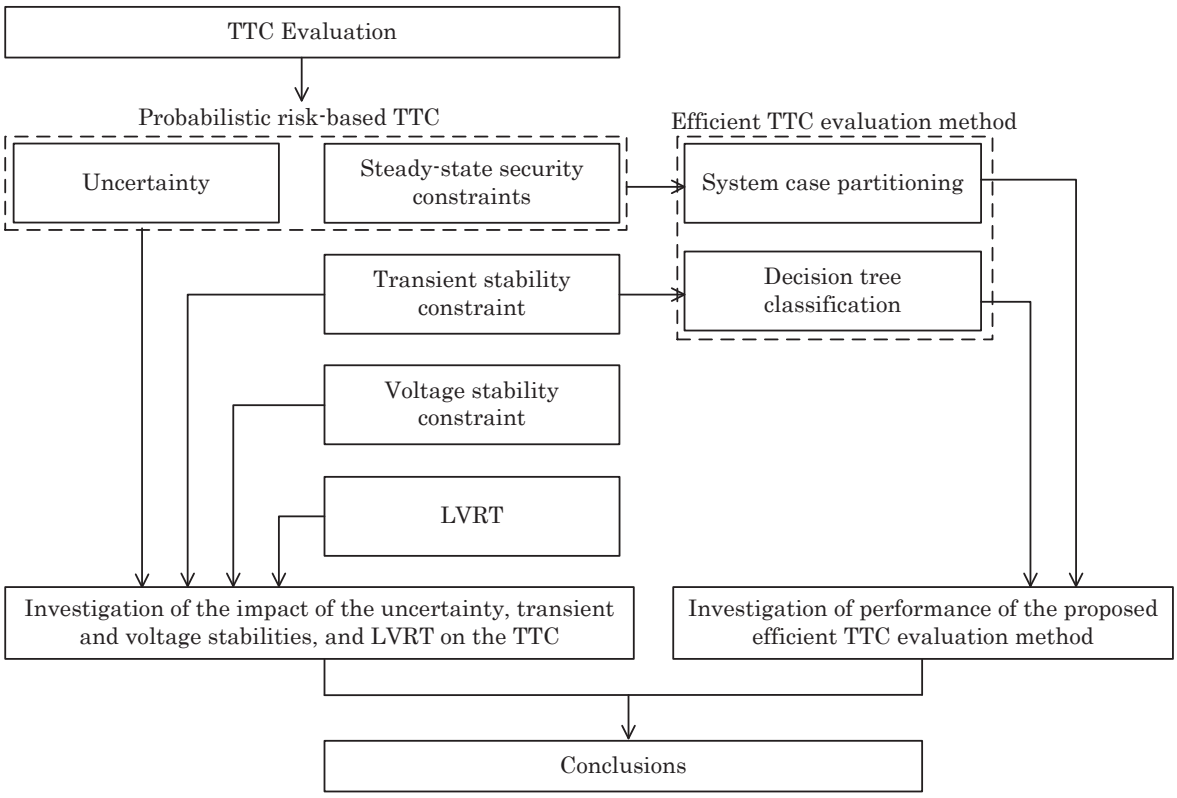

Figure 3: Structure of dissertation.

Chapter 1: Introduction

Chapter 2: Probabilistic Risk-Based TTC Evaluation

Chapter 3: Renewable Energy Modeling

Chapter 4: Efficient TTC Evaluation Method

Chapter 5: Numerical Examples and Results

Chapter 6: Conclusions

Chapter 2

Probabilistic Risk-Based TTC Evaluation

2.1 Introduction

Fast-growing development of renewable energy requires a new method suitable to address the uncertainty associated with its variable power output. The uncertainty may pose an undesirable impact on the system security, hence also on the TTC. This results in a number of literatures on the probabilistic approach for the TTC evaluation reported up to present [5]–[9]. One of the commonly used techniques is Monte Carlo simulation due mainly to its flexibility and effectiveness in dealing with various kinds of uncertainty associated with the operation of a power system ranging from forecast data to equipment availability.

Based on the probabilistic approach, not only the base-case operating condition but also a number of system cases including system contingencies are considered. A significant number of transmission contingencies are evaluated to ensure the system security under such circumstances. Each system case corresponds to each system operating condition which is based on several uncertain factors as follows:

1. Customer demand
2. Generation output from renewable energy sources
3. System contingencies
4. System component failure

The following sections provide detailed descriptions of the algorithm of the proposed probabilistic risk-based TTC evaluation using the Monte Carlo method, and a scheme to include voltage and transient stabilities into the TTC evaluation. The voltage stability is taken into account by ensuring a margin away from the voltage collapse point. The concept of voltage stability index is presented as it is applied to help screen out the cases prone to voltage instability. Transient stability is assessed by the time-domain simulation to check whether the system can stably move from pre- to post-disturbance condition. Finally, the TTC evaluation with Low Voltage Ride-Through (LVRT) consideration is described.

2.2 Probabilistic Risk-Based TTC Evaluation

The Monte Carlo method is a designation for a stochastic simulation using random numbers. Applications of the Monte Carlo method can be found in many areas including power system engineering, e.g. reliability evaluation. The fundamental concept of the Monte Carlo method is based on repetitively conducting an experiment to collect the result samples, i.e. conducting a sampling simulation. Therefore, the TTC evaluation using the Monte Carlo method is basically based on computer simulation of the operation of a system under a specific set of assumed operating conditions. There are 3 main steps as summarized in Figure 4, and each of which will be described in detail in the following subsections.

1. System case generation
2. MTC calculation
3. System contingencies
4. Risk-based TTC selection from the PDF of the MTC

2.2.1 System Case Generation

Applying the Monte Carlo method to the TTC evaluation, the uncertainty of the system conditions and parameters can be easily taken into account. This technique has been well reported in many TTC literatures. The TTC evaluation is usually performed offline in advance, e.g. a day ahead. Therefore, some of the parameters used in the simulation are the projected or forecast data which inevitably contain some errors. This research considers the uncertainty associated with the following:

1. Forecast demand
2. Forecast power output from wind and PV power generation
3. Equipment availability
4. Fault location

The forecast demand, PV power output and wind power output are obtained from the forecasting process. These forecast parameters are subject to uncertainty as previously mentioned. The characteristics of this uncertainty can be modeled by either typical probability distributions or, if available, those obtained from actual historical statistical data. In this paper, the forecast demand and forecast PV power output are assumed to have a normal probability distribution. A normal probability distribution, sometimes called Gaussian probability distribution, is mathematically expressed as

$$f(x) = \frac{1}{\sigma\sqrt{2\pi}}\exp\left(\frac{-(x-\mu)^2}{2\sigma^2}\right) \tag{2.1}$$

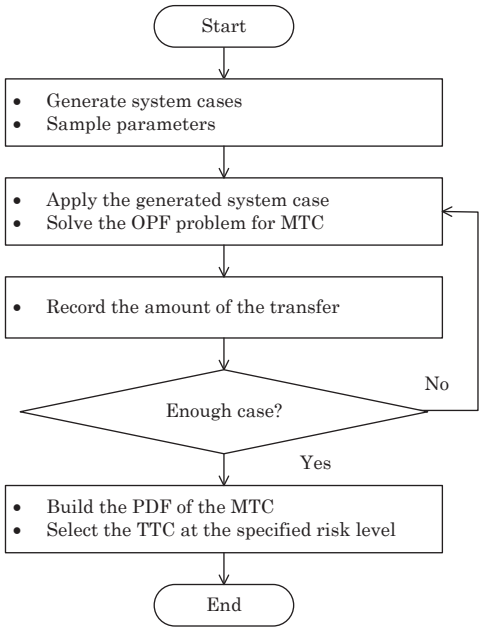

Figure 4: Probabilistic risk-based TTC evaluation flowchart.

where μ is the forecast value, and σ is the standard deviation representing the accuracy of the forecast value.

To sample the parameter, first, a normally distributed random number, z (with zero mean and unity standard deviation) is generated either by the approximate inverse transform method or Box-Müller method. The sampled value is then converted from

$$x = x_\mu + \sigma z \tag{2.2}$$

where x and x_μ are the sampled and forecast values.

On the contrary, the probability distribution of the short-term wind power forecast changes with the amount of the power output. Based on the statistical analysis of wind power forecast error described in [19], a Beta distribution rather than a normal distribution can more accurately approximate the short-term wind power forecast. The Beta distribution is given by the following equations:

$$f(x, \alpha, \beta) = \frac{1}{B(\alpha, \beta)} x^{\alpha-1}(1-x)^{\beta-1} \tag{2.3}$$

$$B(\alpha, \beta) = \int_0^1 x^{\alpha-1}(1-x)^{\beta-1} dx \tag{2.4}$$

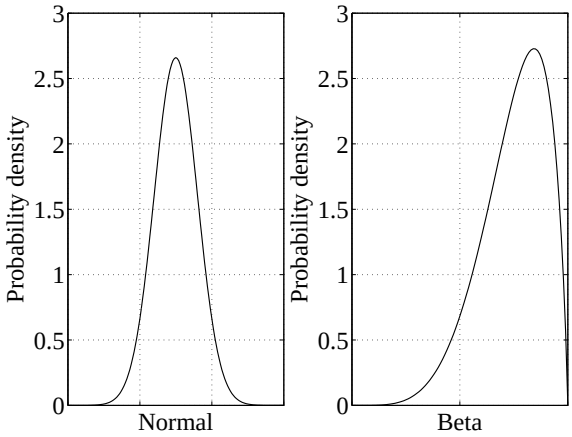

Figure 5: Comparison between Normal and Beta distributions.

Here $B(\alpha, \beta)$ is the Beta function, and α, β are parameters related to the mean, μ, and variance, σ^2 as follows:

$$\mu = \frac{\alpha}{\alpha + \beta} \tag{2.5}$$

$$\sigma^2 = \frac{\alpha\beta}{(\alpha + \beta)^2(\alpha + \beta + 1)} \tag{2.6}$$

A Beta distributed random number, b is generated from

$$b(\alpha, \beta) = \frac{g(\alpha)}{g(\beta) + g(\alpha)} \tag{2.7}$$

where g is a Gamma distributed random number which is generated from

$$g(\gamma) = -\ln \prod_{i=1}^{\gamma} U_i \tag{2.8}$$

where γ is the shape parameter, and U_i is a uniform random number within [0,1].

Figure 5 shows the comparative plot between normal and Beta distributions. The uncertainty degree of the parameters, i.e. the accuracy of the forecast, is specified by a standard deviation expressed in percent of the forecast value. The larger the standard deviation the higher the uncertainty degree. This is analogous to shaping the distribution. In general, the accuracy of the forecast depends on several factors, e.g. the forecast techniques, system characteristics, geographical locations, climatic patterns, etc. Availability status of the equipment, i.e. a transmission line is determined from a state sampling method [20] with the use of historical reliability data. Therefore, the unavailability of a transmission line represents a contingency condition due to disturbances, i.e. an outage case.

Table 1: Probability of a fault location

Line segment	Probability
Near-ended	0.1307
Middle	0.7021
Far-ended	0.1672

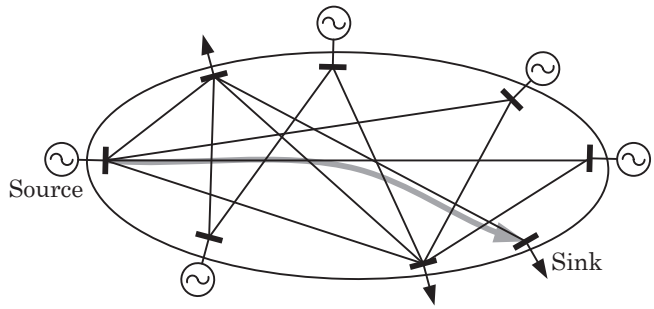

Figure 6: Point-to-point transfer.

Finally, the fault location on the faulted element is also uncertain. To give an example, a fault on a transmission line can occur at any position along the line. Generally, the fault location on a line generally does not follow a uniform distribution. It rather occurs at the middle of the line than at the two ends. Therefore, this research applies a discrete probability distribution adopted from [21]. A transmission line is divided into 3 segments: Near-ended (first 20% of the line), Middle (middle 60% of the line), and Far-ended (last 20% of the line). Each segment has the probability of fault occurrences estimated from the historical reliability data as tabulated in Table 1. The sampling is done by first generating a uniform distributed random number within the range between 0 and 1. As a result, the value of the random number simply indicates at which segment the fault occurs.

2.2.2 MTC Calculation

Maximum Transfer Capability (MTC) can be obtained by solving the optimization problem in which the power transfer is maximized, as mentioned in Chapter 1. The details of the formulation of the OPF problem will be explained again in this subsection. In this research, the MTC is evaluated for a point-to-point transfer of the interested path as depicted in Figure 6. MTC can be obtained by increasing the generation at the source bus and load at the sink bus. The amount of additional load is specified here by the parameter, λ. The active and reactive loads at the sink bus are modified as follows:

$$P_D = P_D^0 + \lambda \cos(\psi^0) \tag{2.9}$$

$$Q_D = Q_D^0 + \lambda \sin(\psi^0) \tag{2.10}$$

where P_D, Q_D are active and reactive loads at the sink bus; P_D^0, Q_D^0 are base-case active and reactive loads at the sink bus; ψ^0 is the base-case power factor angle of the sink bus.

This problem can be formulated as an OPF problem with the objective function to maximize the transfer by maximizing λ.

$$\left.\begin{array}{l} \max \quad \lambda \\ \text{s.t.} \\ G(x,\lambda) = 0 \\ H(x,\lambda) \leq 0 \end{array}\right\} \tag{2.11}$$

where x is a vector of system control and state variables, $G(x,\lambda)$ are a set of equality constraints representing the power balance equations, and $H(x,\lambda)$ are a set of inequality constraints representing system security limits. In general, the transfer capability is restricted by the following limits:

1. Voltage magnitude limit
2. Generation capacity limit both active and reactive power
3. Equipment thermal limit
4. Transient stability limit
5. Voltage stability limit

The first three limits can be directly incorporated into the optimization problem. On the other hand, the security limits related to transient and voltage stabilities are taken into account separately which will be described in the next sections. Nonetheless, in some literatures, the transient stability constraint is simply taken into account by imposing the bus voltage angle limit into the set of the inequality constraints. The use of this static constraint to account for the transient stability is simple but not always reliable. Once the maximum λ is successfully solved, the MTC is computed from

$$MTC = P_D^0 + \lambda_{\max} \cos(\psi^0). \tag{2.12}$$

The OPF problem as formulated in Eqs. (2.9)–(2.11) can be solved by a number of methods, e.g. heuristic-based methods such as evolutionary programming, particle swamp optimization technique, or classic gradient-based methods such as Sequential Quadratic Programming (SQP). This research simply uses SQP, a suitable method for solving constrained nonlinear problems. The SQP algorithm reduces the original optimization problem into a quadratic programming sub-problem which is later solved based on the Kuhn-Tucker conditions (please see the appendix for more detailed descriptions).

2.2.3 Risk-Based TTC Selection

In the past, the TTC was simply selected from the minimum MTC within a set of specified system conditions, e.g. N-1 contingencies.

$$TTC = \min \{MTC_1,\ MTC_2, ..., MTC_N\}\,. \tag{2.13}$$

Here N is a set of system conditions. This selection scheme is conservative and reflects no stochastic nature of the system. In addition, the TTC is often masked by the severe system condition which usually has a small probability of occurrence; hence, it may not occur within the specified lead-time. This is to emphasize that this method fails to consider the probabilistic nature of a power system. Furthermore, not only the N-1 contingencies but also several of the N-2 contingencies are of importance. With this regard, a more appropriate way is to select the TTC based on the probabilistic approach.

This risk-based TTC selection relies on the probabilistic concept in which the TTC is selected from the probability density function (PDF) of the MTC obtained from Monte Carlo simulation. The PDF of the MTC is constructed once the MTC's of all generated system cases are attained. The risk refers to the chance that the system fails to conduct the transfer at the specified value, i.e. the accumulated probability of the cases having the MTC smaller than the specified transfer, the shaded area shown in Figure 7. The specified risk, in general, varies from system to system depending on the security requirement. The optimal risk can also be determined from the benefit and risk analysis [7].

To give an example, the TTC at 5% risk means that when setting the TTC at this value, there is 95% chance based on the statistical analysis that the system will successfully conduct the transfer, i.e. 5% chance to fail. This is one of the advantages of Monte Carlo simulation that it provides additional statistical information which can be used for further analysis.

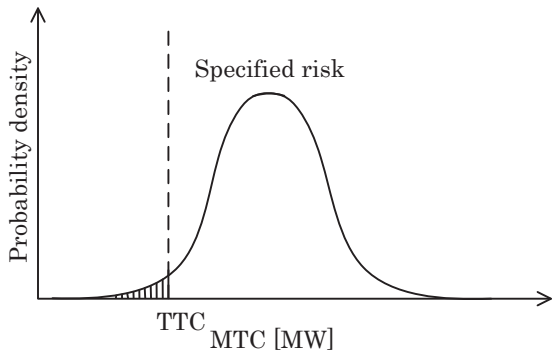

Figure 7: Risk-based TTC selection.

2.3 Voltage Stability Consideration

2.3.1 Background

As always one of the important issues in the planning and operation of a power system, the terms voltage stability and voltage collapse appear frequently in the literatures and discussions of power system planning and operation.

Voltage stability is the ability of a power system to maintain steady acceptable voltages at all buses in the system under normal operating conditions and after being subjected to a disturbance. Voltage instability is essentially a local phenomenon; nonetheless, its consequences may have a widespread impact. On the other hand, voltage collapse is more complex than simple voltage instability and it is usually the result of a sequence of events accompanying voltage instability leading to a low-voltage profile in a significant part of a power system.

Voltage instability normally occurs in a heavily stressed power system, leading to voltage collapse aforementioned, undesirable blackouts, and economical loss. Such stressed conditions are commonly associated with the stressed load and contingencies e.g. loss of a large generation or transmission facilities, or gradual loss of synchronism of machines. In recent years, voltage instability has been responsible for several major network collapses. Several examples of them are [22]:

1. New York power pool disturbances of September 22, 1970
2. Florida system disturbance of December 28, 1982
3. French system disturbances of December 19, 1978, and January 12, 1987
4. Northern Belgium system disturbance of August 4, 1982
5. Japanese system disturbance of July 23, 1987

For the TTC evaluation, it is also important to incorporate the voltage stability into the analysis. From the system operator point of view, a quantitative index which indicates how far the current operating point is away from the collapse point can be very useful for the operation. Therefore, this research adopts a voltage stability index to fulfill this task.

This section will begin with the derivation of the voltage stability index. Simple numerical simulations are conducted for verification. Finally, this section summarizes a method to incorporate the voltage stability index into the TTC evaluation.

2.3.2 Voltage Stability Index

The voltage stability index is used to predict the occurrence of the voltage collapse by quantitatively indicating the proximity to the voltage collapse point. In general, the voltage stability index can be derived from a bus or line model. The voltage stability index used in this research is derived from a line model [23]. The mathematical derivation is simply based on the criterion

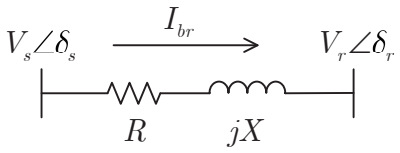

Figure 8: Line connecting two buses.

of the term under the root of a quadratic equation to be greater than zero. When this term is smaller than zero, it causes the roots of the power quadratic equation to be a complex number, which in turn, corresponds to the voltage instability. Consider a line connecting two buses as depicted in Figure 8. In Figure 8, V_s, V_r are the voltage magnitudes at the sending and receiving buses; δ_s, δ_r are the voltage angles at the sending and receiving buses; R, X are the transmission line resistance and reactance; and I_{br} is the line current which is computed from

$$I_{br} = \frac{V_s\angle\delta_s - V_r\angle\delta_r}{R + jX}. \tag{2.14}$$

Considering the complex power at the receiving bus, the following equation is obtained.

$$\frac{V_s\angle\delta_s - V_r\angle\delta_r}{R + jX} = \frac{P_r - jQ_r}{V_r\angle - \delta_r}. \tag{2.15}$$

Separating the real and imaginary parts of Eq. (2.15) gives

$$V_sV_r\cos(\delta_s - \delta_r) - V_r^2 = P_rR + Q_rX \tag{2.16}$$

$$V_sV_r\sin(\delta_s - \delta_r) = P_rX - Q_rR. \tag{2.17}$$

Rearranging Eq. (2.17) for P_r and substituting it into Eq. (2.16) yield a quadratic equation of V_r as

$$V_r^2 + \left(\frac{R}{X}\sin(\delta_s - \delta_r) - \cos(\delta_s - \delta_r)\right) V_sV_r + \left(\frac{R^2 + X^2}{X}\right) Q_r = 0. \tag{2.18}$$

Equation (2.18) can be compared to a standard form, i.e. $aV_r^2 + bV_r + c = 0$ where $a = 1$, $b = \left(\frac{R}{X}\sin(\delta_s - \delta_r) - \cos(\delta_s - \delta_r)\right) V_s$, and $c = \left(\frac{R^2+X^2}{X}\right) Q_r$. To obtain real roots for V_r, the condition $b^2 - 4ac \geq 0$ must be satisfied, which corresponds to

$$\frac{4\left(\frac{R^2+X^2}{X}\right) Q_r}{\left(\frac{R}{X}\sin(\delta_s - \delta_r) - \cos(\delta_s - \delta_r)\right)^2 V_s^2} \leq 1. \tag{2.19}$$

The term in Eq. (2.19) is computed for every line in the system, the voltage stability index is then selected from the maximum value.

The value of the voltage stability index close to 1.0 indicates that the particular line is closed to its instability point which may lead to voltage collapse of the entire system. Therefore, to maintain a secure operation, the value of the voltage stability index should be well kept smaller than 1.0.

2.3.3 Verification of the Voltage Stability Index

This subsection presents a simple simulation for the verification of the voltage stability index. This is to ensure that the voltage stability index described in the previous subsection can accurately predict and show the trend of a system as it is approaching the voltage collapse. The simulation is conducted on the modified IEEE 30-bus system integrated with wind power and PV.

Here the value of the voltage stability index is traced as the sink load is increased. The load at the sink bus is increased step-by-step (specified here by a load multiplier, λ) until the system reaches the nose-point, i.e. power flow fails to converge. Basically, when the load is increased, the system becomes more stressed and prone to the voltage instability. Therefore, the voltage stability index is expected to reflect this trend, i.e. it should also increase with the load.

The trace of the voltage stability index and voltage are plotted in Figures 9 and 10 respectively. The voltage stability index at the base-case operating condition is found to be 0.1094. The result shows that the voltage stability index keeps increasing with the sink load until it finally reaches 0.9352 corresponding to the nose-point. Based on the simulation results, the voltage stability index can roughly indicates the proximity to the nose-point as its value increases toward 1 when the system approaches the voltage instability.

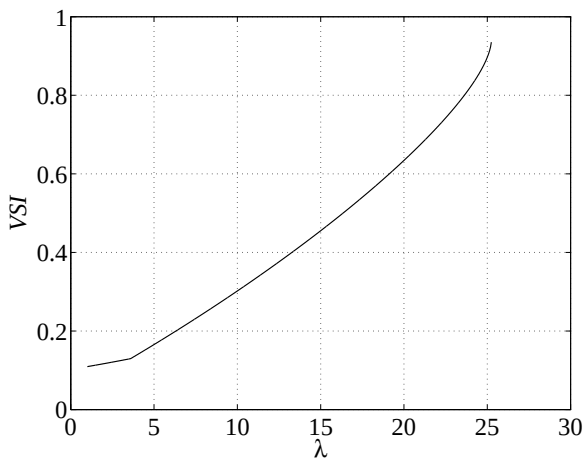

Figure 9: Trace of the voltage stability index as the load increased.

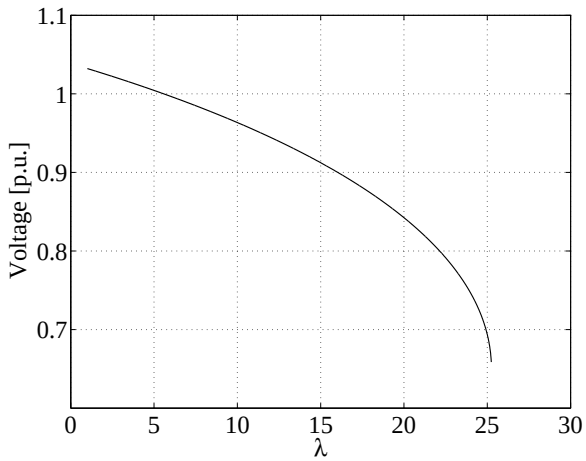

Figure 10: Trace of the voltage as the load increased.

2.3.4 TTC Evaluation with Voltage Stability Consideration

Several literatures directly take into account voltage stability into the TTC evaluation by using a continuation power flow (CPF) [11]. In this method, control parameters are increased in an increment step. The procedure is repeated until the nose-point is reached. CPF solves a set of augmented power flow equations to trace the trajectory of the solution curve passing through the nose-point without encountering numerical difficulty of ill-conditioning. Nonetheless, it is a time-consuming method since the process has to be repeated for a number of system cases during the TTC evaluation. Therefore, this leads to an impetus to search for an alternative means to roughly predict or assess the voltage stability without much computational burden. The hope lies in the voltage stability indices which have been developed for the online voltage stability estimation.

Shown in Figure 11 is the flowchart of the probabilistic TTC evaluation with voltage stability consideration. The voltage stability index is computed after the MTC calculation. If the voltage stability index value is relatively high, compared to a specified threshold value, the margin to the voltage collapse will be checked. The margin to the voltage collapse can be roughly checked by further increasing the sink demand with the specified margin, and then check the convergence of the power flow calculation. If the power flow calculation does not converge, the amount of the transfer is reduced to achieve the voltage stability margin. The adjustment is done in a bi-section manner for a given number of steps.

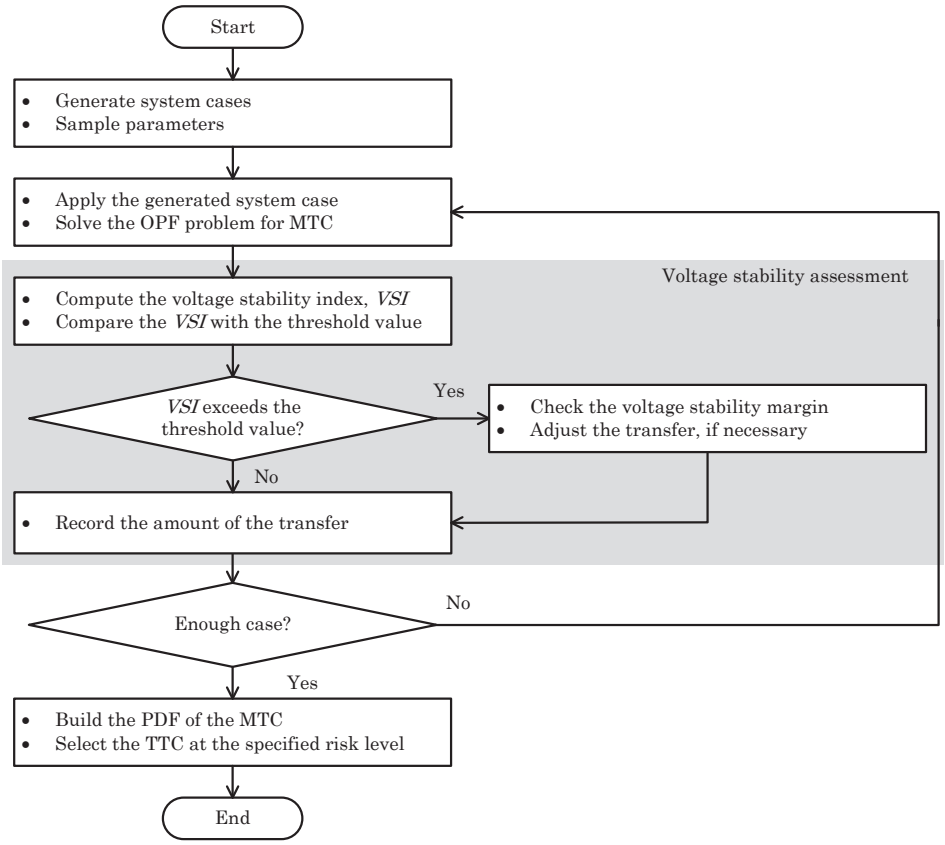

Figure 11: Probabilistic TTC evaluation with voltage stability consideration.

2.4 Transient Stability Consideration

2.4.1 Background

Transient stability is a complex subject that has challenged power system engineers for many years. Transient stability is the ability of a power system to remain in synchronism when subjected to a severe transient disturbance, e.g. a fault on transmission facilities, loss of generation, or loss of large load. The resulting system response involves large excursions of generator rotor angles, bus voltages, and other system variables.

Stability depends on both the initial operating state of the system and the severity of the disturbances. The disturbances can be of several types, e.g. short-circuits of several types: three-phase, phase-to-phase, phase-to-phase-to-ground, or phase-to-ground. In the analysis, they are usually assumed to occur on transmission lines, but occasionally bus or transformer faults are also considered. The fault is assumed to be cleared by the opening of appropriate breakers to isolate the faulted element. The total time required for the relay and breaker operations is termed as the fault clearing time. The analysis of the transient stability can be conducted by means of the time-domain simulation or direct methods. The study period of interest is usually limited to 3 to 5 sec following the disturbance, although it may extend to about 10 sec for very large power systems.

The time-domain simulation solves the nonlinear differential equations describing the generator motions, and other components in the system, by using step-by-step numerical integration techniques, e.g. Euler method, modified Euler method, Runge-Kutta (R-K) method, and implicit integration method based on the trapezoidal rule. They are well collected and described in [22]. This method is the most accurate analysis at present in which the detailed models of generators and other equipment can be included.

In contrast, the direct methods determine the stability without explicitly solving the system differential equations. They instead determine the stability by means of the energy-based methods, i.e. finding the Closest Unstable Equilibrium Point (CUEP). In spite of many accomplishments of the application of the direct methods in recent years, modeling limitations and unreliability of computation techniques continue to be major impediments to their widespread practical use. The direct methods with a sophisticated CUEP solution technique impose heavy computational burden, making it slower than the time-domain simulation.

2.4.2 TTC Evaluation with Transient Stability Consideration

In the TTC evaluation, it is necessary to ensure that such transfer volume can be reliably transferred while satisfying not only static but also dynamic constraints. Incorporating transient stability into the TTC evaluation is one of the most difficult tasks due to the nonlinear characteristics of the power system. A number of literatures simply neglect the transient stability, or adopts a static criterion, e.g. the voltage angle limit. Such criterion is simple but not always reliable. Without considering the transient stability, the obtained TTC is prone to be

optimistic and may not be safe for the practical application. There currently exist two main approaches to incorporate the transient stability into the TTC evaluation.

The first approach attempts to directly incorporate transient stability into the TTC evaluation by imposing a transient stability constraint into the OPF problem commonly termed as TSCOPF [15]. The transient stability constraint is transformed from a set of differential equations approximated by equivalent algebraic equations using the trapezoidal rule. Nonetheless, converting differential equations to algebraic equations may suffer from computational inaccuracy due to the discretizing scheme. In addition, it may lead to a difficulty in convergence particularly for a large power system with a significant number of variables, equations, and contingencies to be incorporated into the optimization problem. Another attempt is to apply the energy function methods as reported in [17], [18]. However, the application of these methods is still limited to a system with only synchronous generators, and no application of these methods to a power system integrated with generation from renewable energy sources has been yet reported.

The other approach is based on an iterative process. The amount of the transfer is iteratively increased, while at the same time, the transient stability is checked, until the system goes unstable. This research adopts this approach. Nonetheless, the main challenge is the computational time which significantly increases due to the addition of the transient stability assessment during the TTC evaluation. The computation burden due to the addition of the transient stability assessment can be alleviated by using decision tree classification which will be described later in Chapter 4.

Shown in Figure 12 is the flowchart of the probabilistic TTC evaluation with transient stability consideration. The procedures are relatively similar to those mentioned in the previous section but with an additional part, i.e. transient stability assessment. For each of the outage scenarios generated from the sampling process, the transient stability is assessed by the time-domain simulation. Starting from the maximum transfer, if the system is unstable, the amount of the transfer is reduced using bisection. This process is repeated until the system is stable or the number of bisection steps is reached.

Whether the transient instability occurs or not is determined from the rotor angle deviation with respect to the center of inertia (COI). The system is said to be stable if the rotor angle deviation of a synchronous generator with respect to COI lies within the allowable range. For wind power generation, it is said to be stable of the induction generator's rotor slip does not exceed the threshold value. The range and threshold value are commonly specified by the utilities which may vary from system to system.

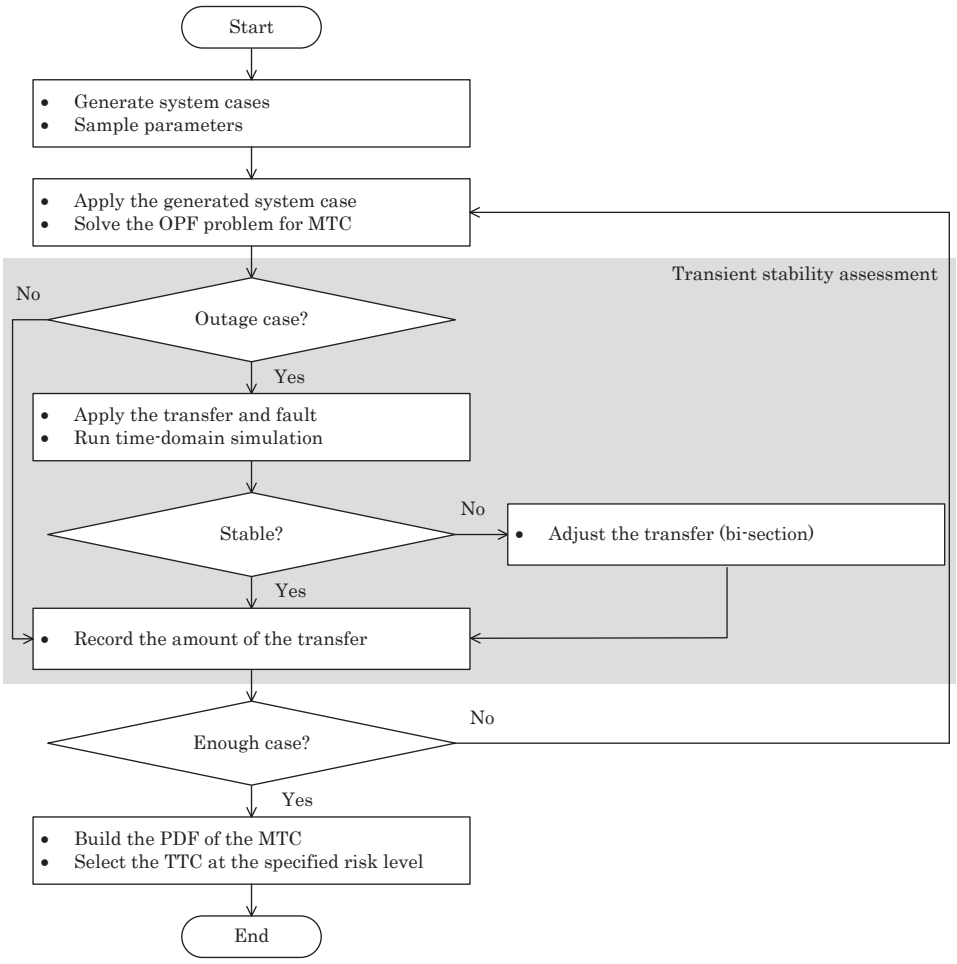

Figure 12: Probabilistic TTC evaluation with transient stability consideration.

2.5 TTC Evaluation with Voltage and Transient Stability Consideration

Finally, putting together both voltage and transient stability considerations into the TTC evaluation gives the following algorithm shown in Figure 13. Here, the voltage stability margin is checked first then followed by transient stability assessment.

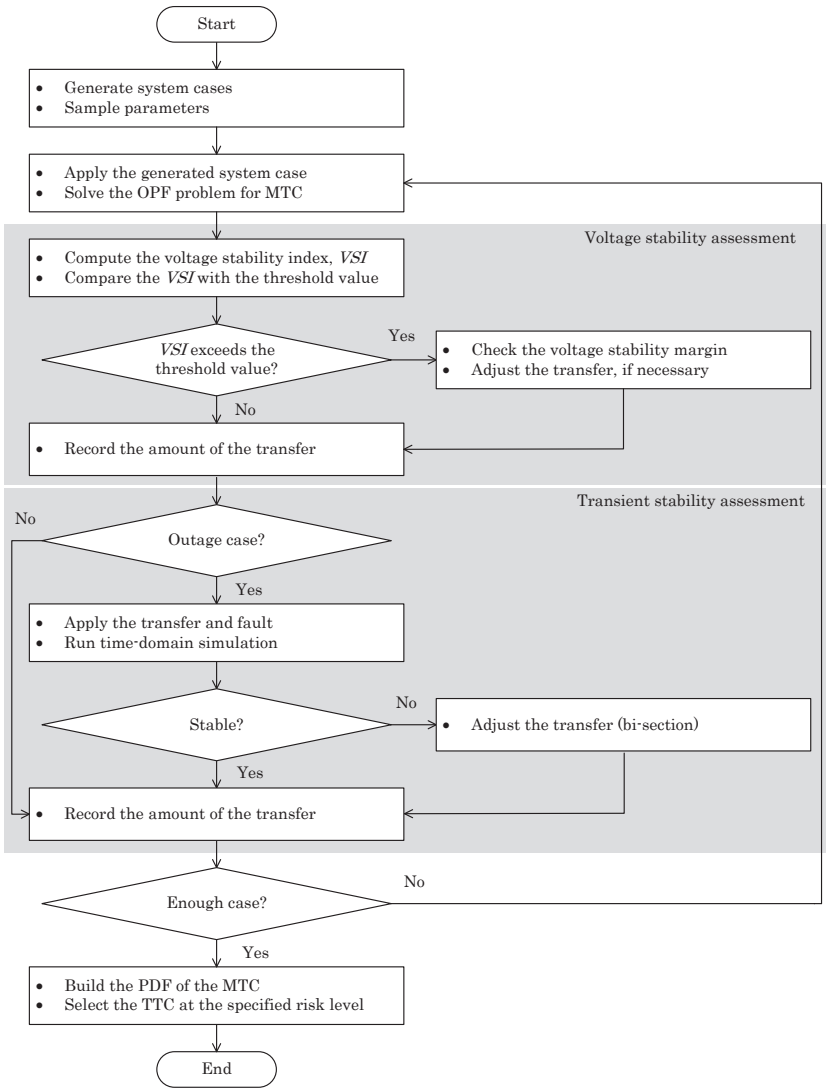

Figure 13: Probabilistic TTC evaluation with voltage and transient stability consideration.

2.6 TTC Evaluation with LVRT Consideration

The number of wind power and PV system installations has grown rapidly worldwide in recent years. This raises a concern that tripping a large generation unit following the disturbance could lead to propagation of transient instability and could potentially cause local or system large-scale blackouts. As a result, this provokes many utilities to adopt Low Voltage Ride-Through (LVRT) requirement for such renewable energy based generating units.

This research so far has assumed that the renewable energy based generating units, e.g. wind farms and photovoltaic (PV) systems are able to remain connected during and following the disturbance regardless of the low voltage. This assumption may not be valid since such generating units are disconnected from the grid when their voltage drops below the specified threshold in order to protect the equipment, e.g. power electronics (an inverter of a PV system) from potential damages due to a high fault current. It is important to note that this research does not aim at formulating the LVRT characteristic requirement or proposing a method to enhance the LVRT capability but only examining the possible impact of the LVRT on system transient stability and TTC.

As is known, disconnecting some generating units is one of the techniques used to improve the transient stability, i.e. reducing the accelerating power. The effectiveness of this technique solely depends on the amount of the generation to be removed. Nonetheless, the loss of large generating units may further risk the stability of the system, contributing to amplification of the effect of the disturbance. As well, this may result in undesirable excursion of the system frequency since the system has to redispatch to make up for the generation lost. The frequency excursion may further lead to system frequency problem or even frequency collapse. This situation raises a concern among utilities as a large-scale renewable energy based generation penetrating into a system.

To avoid the situations where large generating units are disconnected during the fault, system operators have developed voltage and time duration profile which define requirements of a generating unit to ride through the fault without disconnection, i.e. LVRT. In addition, some system operators further require contribution to voltage stabilization and system recovery during and after the fault [24].

In general, LVRT characteristic is defined by the voltage duration profile as depicted in Figure 14. Each point on the curve represents a voltage level and an associated time duration which connected generating units must withstand or ride through. It should be cautioned to note that the profile is not a voltage-time response curve obtained by plotting the transient voltage response. Several LVRT characteristics specified in different grid codes [25] have been reviewed as summarized in Table 2.

In Table 2, U_r is the nominal voltage level. It can be noted that the LVRT characteristic is basically defined by a minimum voltage throughout the duration of the fault followed by a ramping up to nominal level as the voltage recovers. The width of this minimum is dictated by protection technologies and fault clearing time (usually 10 to 20 cycles). On the other hand,

Table 2: Summary of the LVRT characteristics

TSO	Fault duration [sec]	$V_{\min}$ [% of U_r]	Recovery time
AESO	0.625	15	90% after 3 sec
EIRGRID	0.625	15	90% after 3 sec
FERC	0.625 or 0.15	15 or 0	90% after 3 sec
Hydro-Quebec	0.15	0	90% after 3 sec
Scottish Power	0.14 or 0.1	0	80% after 1.2 sec
PSE	0.625	15	80% after 3 sec
WECC	0.15	0	90% after 1.75 sec

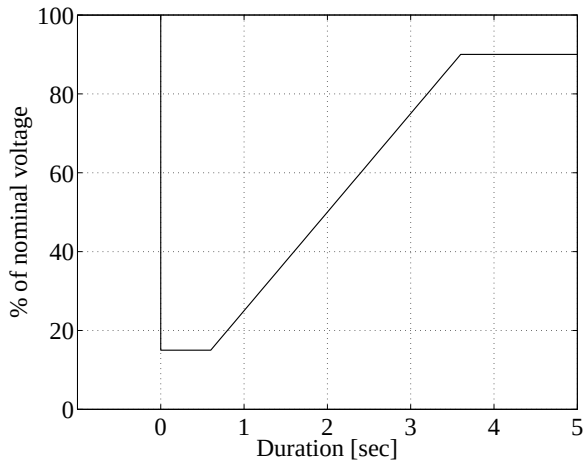

Figure 14: Example of voltage duration profile.

the recovery slope is dictated by the strength of the system and reactive power support.

For the TTC evaluation, the assumption that all generating units are able to remain connected during after the fault may not be valid. Some of them may not be able to comply with the requirement in case of a very severe fault condition. Therefore, this research first examines the possible impact of LVRT consideration on the transient stability and discovers what factors related to the disconnection degrade the transient stability. Given a LVRT characteristic, if voltage response at the terminal of a generating unit fails to comply with the duration profile, the generating unit will be disconnected.

Another point to be examined is how much LVRT consideration could affect the TTC. Due to the stochastic nature of the fault itself, such severe fault which causes a significant drop in the system voltage; hence, a number of generating units are tripped, may not occur frequently or does not occur at all within the specified lead-time. Although its consequences are significant, it may not impose much impact on the TTC.

Chapter 3

Renewable Energy Modeling

3.1 Introduction

Recently, it can be witnessed rising environmental concerns, e.g. greenhouse gas emission, and cost escalation associated with conventional energies used for electricity production. These factors have led to a major impetus to the utilization of renewable energy sources for electricity production. This trend is also expected to continue with more and more generation from renewable energy sources in a form of distributed generation penetrating into a power system. Among several renewable energy sources available technologies, wind power and photovoltaic (PV) have received a great attention worldwide and been the most developed.

The IEA's World Energy Outlook 2004 forecasts that the global share of renewable energy in electricity generation will increase to 19% by 2030. EU and North America are among the world leading countries in renewable energy development and have launched wind power development projects of 120 GW and 305 GW by 2030 respectively. In contrast, Japan ranked the 13th in the world in 2008 with a cumulative 1860 MW wind capacity. Japanese government has also set out a target for wind power development of 6610 MW and 53 GW PV power development by 2030 [26].

Renewable energy can make major contributions to the diversity and security of energy supply, to economic development, and to addressing local environmental pollution. In addition, considerable attention has been attracted to its potential to address global warming through zero or near zero net greenhouse gas emissions. Although renewable energy offers a great appeal and several advantages, a large penetration of this renewable energy based generation may cause unfavorable impact on the system security and reliability such as reverse power flow, voltage problem, excess power, frequency fluctuation, etc. The impact was simply ignored in the past since the installed capacity was not large enough; hence, the impact was minor. Nonetheless, as more renewable energy is penetrating into a power system, the impact becomes significant and cannot be simply overlooked. Therefore, such impact on the system transfer capability is also expected and should be examined and included in the TTC evaluation.

This research considers two types of the renewable energy based generation, i.e. wind power and PV. They have been the most developed among various renewable technologies with a large penetration expected within the near future. Their modeling for the steady-state and dynamic analyses is based on an aggregated model in order to reduce the complexity and problem dimension. Detailed descriptions are given in the following sections.

3.2 Wind Power Modeling

3.2.1 Steady-State Model

The working principle of a wind turbine encompasses two conversion processes. First, the turbine extracts the kinetic energy of the wind and converts it into a mechanical torque. This mechanical torque applies to a rotor of a generating unit, typically an induction generator, to produce electricity. Although there are currently several wind turbine technologies, this research deals only with a constant speed wind turbine technology with a squirrel induction generator (SCIG). This is because this type of wind power generator has a more severe impact on the transient and voltage stabilities than the other types. The configuration of a wind power system with a constant speed wind turbine is depicted in Figure 15. It consists of a conventional squirrel cage induction generator directly connected to the grid. The slip, hence the rotor speed of a squirrel cage induction generator varies with the amount of the generated power. Generally, this rotor speed variation is rather small, i.e. approximately within the range of 1–2 percent. A squirrel cage induction generator always consumes reactive power for its magnetization. This is undesirable, especially when connected to a weak power grid. Therefore, the reactive power demand is compensated from a series of capacitor banks in order to keep the power factor close to one.

The conversion of mechanical power of the wind turbine into electrical power is usually accomplished by an induction generator. Therefore, to assess the impact of wind power generation, an adequate modeling of an induction generator is required. In many literatures, an induction generator is commonly modeled as a PQ bus [8], [27]. That is, the active power generation is assumed to be known with a given power factor from which the reactive power is calculated. Although this model is simple to be incorporated into the analysis, the accuracy is not so satisfactory. The accuracy can be improved by taking into account a steady-state model of an induction generator as shown in Figure 16.

Usually, only the forecast wind power output and induction machine's parameters are available. The other related parameters, i.e. terminal voltage, consumed reactive power, and rotor slip are computed from the modified power flow problem. The power balance equations of the bus i connected to the wind power generation are modified to include the complex power terms of the wind power generation as written in Eqs. (3.1)–(3.2). Due to the addition of a new variable, i.e. a rotor slip, another equation is required for solving the power flow problem. Equation (3.3) enforces the wind power output to its specified or forecast value.

$$f_{Pi} = F_{Pi}(\delta, V) - P_{Wi}^{\text{spec}} + P_{Di} = 0 \tag{3.1}$$

$$f_{Qi} = F_{Qi}(\delta, V) + Q_{Di} + Q_{Wi}(V_i, s_i) = 0 \tag{3.2}$$

$$f_{P_W i} = -P_{Wi}(V_i, s_i) - P_{Wi}^{\text{spec}} = 0 \tag{3.3}$$

where

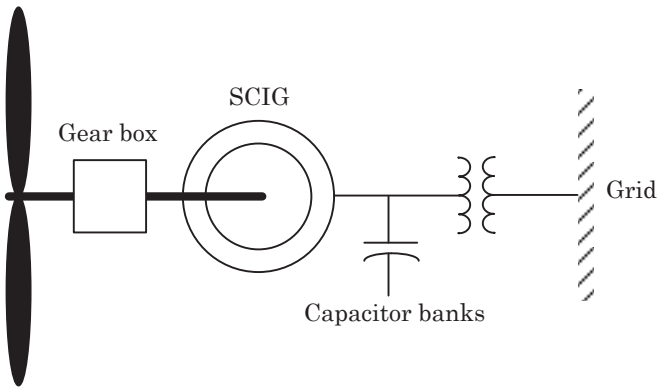

Figure 15: Wind power generation.

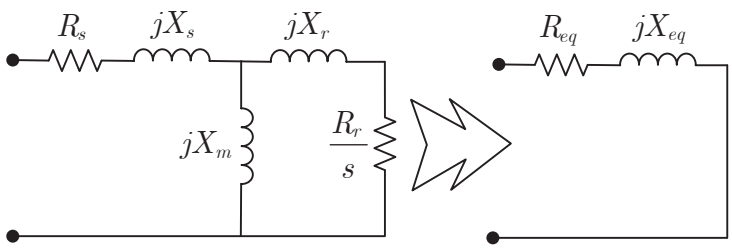

Figure 16: Steady-state induction generator circuit.

$$P_{Wi}(V_i, s_i) = \frac{V_i^2}{R_{eq}^2(s_i) + X_{eq}^2(s_i)} R_{eq}(s_i)$$

$$Q_{Wi}(V_i, s_i) = \frac{V_i^2}{R_{eq}^2(s_i) + X_{eq}^2(s_i)} X_{eq}(s_i)$$

$$F_{Pi}(\delta, V) = \sum_{j=1}^{N} V_i V_j (G_{ij} \cos \delta_{ij} + B_{ij} \sin \delta_{ij})$$

$$F_{Qi}(\delta, V) = \sum_{j=1}^{N} V_i V_j (G_{ij} \sin \delta_{ij} - B_{ij} \cos \delta_{ij}).$$

Here P_{Wi} and Q_{Wi} are the active and reactive power terms of the wind power generation expressed using load convention; P_{Wi}^{spec} is the specified or forecast wind power output; G_{ij} and B_{ij} are the real and imaginary parts of the ij^{th} element in the admittance matrix; V_i and V_j are the voltage magnitudes at buses i and j respectively; δ_{ij} is the voltage angle difference between

buses i and j; and N is the number of buses. In Eqs. (3.4)–(3.5), R_{eq}, X_{eq} are the equivalent resistance and reactance derived from a steady-state circuit of an induction generator as shown in Figure 16. In Figure 16, R_s, R_r are the stator and rotor resistances; X_s, X_r are the stator and rotor reactances; X_m is the magnetizing reactance; and s is the rotor slip.

$$R_{eq} = \frac{\frac{R_r X_m^2}{s}}{(\frac{R_r}{s})^2 + (X_m + X_r)^2} \tag{3.4}$$

$$X_{eq} = \frac{(\frac{R_r}{s})^2 X_m + X_m X_r (X_m + X_r)}{(\frac{R_r}{s})^2 + (X_m + X_r)^2} \tag{3.5}$$

If there are N_W induction generators connected to the system, there will be N_W additional variables (i.e. rotor slips) and N_W additional equations. This modified power flow problem can also be solved by Newton Raphson's method with the update step expressed in the following equation.

$$\begin{bmatrix} \frac{\partial f_P}{\partial \delta} & \frac{\partial f_P}{\partial V} & \frac{\partial f_P}{\partial s} \\ \frac{\partial f_Q}{\partial \delta} & \frac{\partial f_Q}{\partial V} & \frac{\partial f_Q}{\partial s} \\ \frac{\partial f_{P_W}}{\partial \delta} & \frac{\partial f_{P_W}}{\partial V} & \frac{\partial f_{P_W}}{\partial s} \end{bmatrix} \begin{bmatrix} \Delta\delta \\ \Delta V \\ \Delta s \end{bmatrix} = \begin{bmatrix} \Delta f_P \\ \Delta f_Q \\ \Delta f_{P_W} \end{bmatrix} \tag{3.6}$$

3.2.2 Dynamic Model

The mechanical input power from the wind is applied to the shaft model, i.e. the drive train, which drives the rotor of an induction generator. Note that the time-frame of the transient stability analysis is rather short; as a result, it is common to neglect the rotor model by assuming that the wind speed is constant over the period of study. This is equivalent to a constant mechanical input power throughout the simulation. The dynamic model of wind power generation is based on an aggregated two-mass model [28]. Neglecting the shaft damping, the differential equations describing the motion of the two rotating parts, i.e. wind turbine and induction generator rotors, are as follows:

$$\frac{d\omega_{wr}}{dt} = \frac{T_{wr} - K_s\gamma}{2H_{wr}} \tag{3.7}$$

$$\frac{d\omega_m}{dt} = \frac{K_s\gamma - T_e}{2H_m} \tag{3.8}$$

$$\frac{d\gamma}{dt} = 2\pi f_0(\omega_{wr} - \omega_m) \tag{3.9}$$

where f_0 is the system frequency base; T_{wr}, T_e are the turbine rotor and induction generator electrical torques; γ is the angular displacement between the two ends of the shaft; ω_{wr}, ω_m are the rotational speeds of the turbine rotor and induction generator rotor; H_{wr}, H_m are the inertia constants of the turbine rotor and induction generator; K_s is the shaft stiffness.

Following are a set of differential equations associated with an induction generator in a d-q reference frame expressed using generator convention.

$$\frac{dv_d^{'}}{dt} = -\frac{1}{T_0^{'}}\left(v_d^{'} - (X_s - X_s^{'})i_{qs}\right) + s\omega_s v_q^{'} \tag{3.10}$$

$$\frac{dv_q^{'}}{dt} = -\frac{1}{T_0^{'}}\left(v_q^{'} + (X_s - X_s^{'})i_{ds}\right) - s\omega_s v_d^{'} \tag{3.11}$$

where

$$v_{ds} = -R_s i_{ds} + X_s^{'} i_{qs} + v_d^{'}$$
$$v_{qs} = -R_s i_{qs} - X_s^{'} i_{ds} + v_q^{'}$$
$$s = \frac{\omega_s - \omega_m}{\omega_s}.$$

Here v_{ds}, v_{qs} are d-axis and q-axis stator voltages; $v_d^{'}$, $v_q^{'}$ are d-axis and q-axis transient voltages; i_{ds}, i_{qs} are d-axis and q-axis stator currents; R_s, X_s, $X_s^{'}$ are machine resistance, stator leakage and transient reactances; $T_0^{'}$ is the rotor time-constant; ω_s is a synchronous rotational speed.

3.3 Photovoltaic (PV) System Modeling

3.3.1 Steady-State Model

The photovoltaic (PV) power technology uses semiconductor cells to convert solar energy to electrical energy. In the past, PV applications have been limited to remote locations not connected to the utility grid or isolated regions. With the declining price and improvements in manufacturing, this sector is expected to grow and play a significant role in the future electricity production. The United States, Japan, India, China, and other countries have launched new programs to increase the installation capacity within the near future.

The configuration of a typical PV system includes a number of PV arrays connected to a power conditioning unit, i.e. an inverter, which converts the DC power to AC power and feed it to the grid. Both active and reactive power can be controlled via the inverter control, i.e. a power regulator. The reactive power is usually controlled to keep the power factor within a specified range, while the active power is controlled to achieve the maximum power. A typical grid-connected PV system is depicted in Figure 17.

For the steady-state analysis, e.g. power flow and optimal power flow calculation, due to the ability to regulate the reactive power fed to the grid via the inverter control, the bus connected to the PV system is simply modeled as a PQ (i.e. load) bus operating at a unity power factor. The generation is conceived as a negative load.

3.3.2 Dynamic Model

The PV dynamic model used here is highly simplified. The power conditioning unit of a PV system is modeled as a current source [29]. The current is controlled to achieve the active and reactive power reference set-points, i.e. P_{ref} and Q_{ref}. The power regulator is simply a PI controller as shown in Figure 18. It is assumed that the inverter can adjust its current with the time delay T of 0.01 sec fast enough to follow the reference signals from the power regulator.

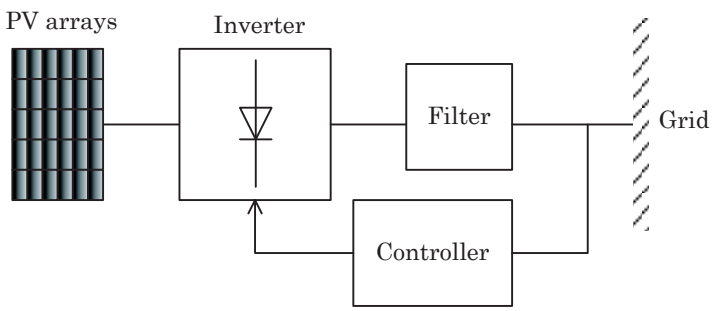

Figure 17: PV system configuration.

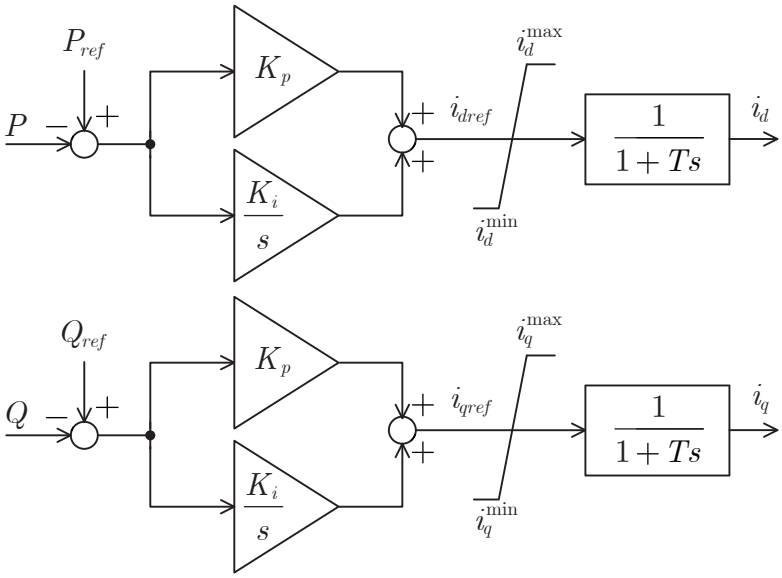

Figure 18: Power regulator of a PV system.

Chapter 4

Efficient TTC Evaluation Method

4.1 Introduction

Consideration of the uncertainty and transient stability constraint considerably adds a computational burden to the TTC evaluation. Monte Carlo simulation usually requires a sufficiently large sample size to ensure the convergence; hence, it is time-consuming. Further, the addition of the time-domain simulation for transient stability assessment requires a significant amount of the run time as a number of outage cases in a given sample set are checked. Therefore, the computational speed may not be fast enough to provide the TTC for the system operators in time. Some literatures propose fast TTC evaluation method using sensitivities or intelligent techniques, e.g. artificial neural network [30]–[32]. However, these methods have limitations making it difficult to include uncertainty into the evaluation. In some studies, network reduction techniques, e.g. extended Ward equivalent [13], REI [33], are applied to find the equivalent network to help speed up the computation. In these reduction techniques, the network is divided into internal and external networks. The internal network is an interested part which needs to be analyzed in detail whereas the remaining is considered to be an external network. Therefore, the external network will be represented by an equivalent network with the size much smaller than the original one. Even though for some TTC applications, e.g. a day ahead TTC, the computational speed is not much a problem, if possible, this research aims to speed up the computation to a level that it can be included into an energy management system, i.e. moving close to a real-time application.

To achieve the target aforementioned, this research proposes two techniques to speed up the TTC computation, i.e. system case partitioning and decision tree classification. Similar to system contingency ranking, system case partitioning is used to reduce the sample size, i.e. the number of samples to be evaluated during Monte Carlo simulation. Decision tree classification is applied here for fast transient stability prediction.

This chapter begins with the concept of system case partitioning describing two filters used to rank the system cases within a given sample set. The first filter employs the performance indices to measure the severity degree related to the static constraints. The second filter uses a decision tree to roughly identify the unstable cases related to the transient stability constraint. Then, the principle of decision tree classification, its growing algorithm based on CART, and how to apply it for transient stability prediction are given. Finally, the framework to apply these two techniques to the TTC evaluation is described.

4.2 System Case Partitioning

As is known, Monte Carlo simulation usually requires a sufficiently large sample size to ensure the convergence; as a result, it is time-consuming. Referring to the risk-based TTC selection described in Chapter 2, it can be noted that not all the system cases are related to the risk, i.e. having small MTC. Therefore, to obtain the TTC, it is not necessary to compute the MTC of all the system cases, only those related to the risk are sufficient. Based on this concept, the system cases will be partitioned into two main groups based on their severity degree; risk-related and non-risk-related groups respectively. Considering only the above partitioned cases, a significant number of the OPF calculations in the Monte Carlo simulation and time-domain simulations in the transient stability assessment can be reduced; as a result, the run time can be saved.

Most of the risk-related cases are severe cases whose transfer is restricted by either steady-state or transient stability constraint. Thus, two filters are used here to screen out such risk-related cases.

Filter 1 is to screen out the risk-related cases due to the steady-state constraints using the performance indices (PI's) [34].

Filter 2 is to screen out the risk-related cases due to the transient stability constraint using a decision tree to predict the system transient stability.

The algorithm of the partitioning process is given in Fig. 19. The system cases from the system case generation are applied to 2 filters. Filter 1 ranks the cases based on the ΔJ_{sys} value in a descending order, i.e. from the most severe (largest ΔJ_{sys}) to the least severe cases (smallest ΔJ_{sys}). At the same time, the stability of the outage cases within the sample set is predicted using Filter 2, i.e. decision tree. The partitioned set is then built by selecting the cases from the results of these 2 filters. Here the results of Filter 2 (i.e. the outage cases classified by Filter 2 as unstable) are included first in the partitioned set and followed by those of Filter 1 (i.e. ranked system cases) until the specified number of cases for the partitioned set is attained.

It should be emphasized here that the proposed risk-based TTC evaluation with system case partitioning differs from a conventional TTC evaluation with contingency screening in that the proposed method starts off with much wider sample space where the uncertainty is fully taken into account. The process is based on a probabilistic method and focuses only on the sample set required to obtain the risk-based TTC value.

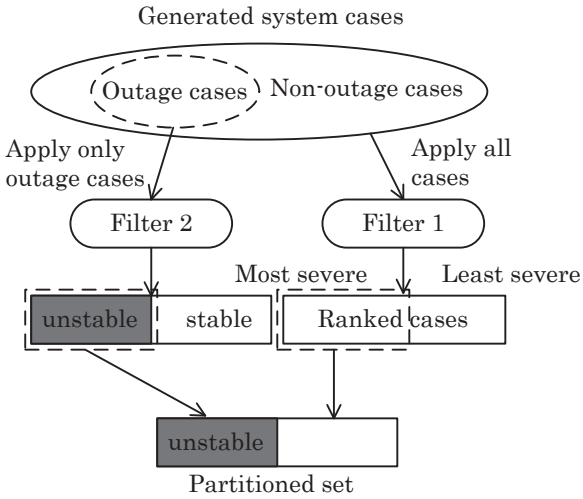

Figure 19: Partitioning process.

4.3 Performance Indices

The performance indices are commonly used in contingency ranking to measure the severity of the system conditions. They are also applied here to rank the system cases within a sample set according to their severity degree.

First, the bus voltage performance index, J_V is given by

$$J_V = \sum_{i=1}^{N_{PQ}} c_{Vi} \left(\frac{V_i - V_{i,\text{mean}}}{V_{i,\text{tol}}} \right)^{2n} \tag{4.1}$$

where $V_{i,\text{mean}}$ is the mean bus voltage, i.e. $0.5(V_i^{\max} + V_i^{\min})$; $V_{i,\text{tol}}$ is the deviation tolerance, i.e. $0.5(V_i^{\max} - V_i^{\min})$; V_i is the voltage at bus i; c_{Vi} is a coefficient; n is a positive integer defining the exponent; N_{PQ} is the total number of PQ buses.

Similarly, the generation reactive power performance index, J_Q is given by

$$J_Q = \sum_{i=1}^{N_G} c_{Qi} \left(\frac{Q_i - Q_{i,\text{mean}}}{Q_{i,\text{tol}}} \right)^{2n} \tag{4.2}$$

where $Q_{i,\text{mean}}$ is the mean generated reactive power, i.e. $0.5(Q_i^{\max}+Q_i^{\min})$; $Q_{i,\text{tol}}$ is the deviation tolerance, i.e. $0.5(Q_i^{\max} - Q_i^{\min})$; Q_i is the generated reactive power by a generator i; c_{Qi} is a coefficient; n is a positive integer defining the exponent; N_G is the total number of generators.

The branch flow performance index, J_S is given by

$$J_S = \sum_{i=1}^{N_{br}} c_{Si} \left(\frac{S_i}{S_i^{\max}} \right)^{2n} \tag{4.3}$$

where S_i is the apparent power flow of the branch i; $S_i^{\max}$ is the thermal rating; c_{Si} is a coefficient; n is a positive integer defining the exponent; N_{br} is the total number of branches.

Finally, the system performance index, J_{sys} can be obtained from

$$J_{sys} = \frac{w_V J_V + w_Q J_Q + w_S J_S}{w_V + w_Q + w_S} \tag{4.4}$$

where w_V, w_Q, w_S are the weighting factors. They are equally set to 1 in this research.

Note that the performance index, J is a function of the state variables, i.e. $J(x)$. The state variables change as the system condition changes due to the uncertainty, outages, and addition of the transfer. Therefore, the severity of the system cases can be ranked according to the change of the system performance index value as follows:

$$\Delta J_{sys} = J_{sys}(x) - J_{sys}(x_0) \tag{4.5}$$

where x_0 and x are the vectors of state variables prior to and after the system condition change respectively.

The coefficients in Eqs. (4.1)–(4.3), c_{Vi}, c_{Qi}, c_{Si} are 1 if the system condition after the system condition change is more severe than the base-case condition; and 0 otherwise. Here, the exponent n is set to 4 which is found large enough to avoid the masking problem. The algorithm for system case ranking is summarized as follows:

1. Run power flow at the base-case condition, and find the base-case MTC.
2. Apply the system condition change, i.e. change of demand, renewable energy power output, system configuration, and add the transfer, here set to 75% of the base-case MTC. This addition of the transfer helps specify the direction where the system will move from the base-case condition; hence, the constraint which limits the transfer can be predicted as depicted in Figure 20.
3. Run power flow for the system condition after the system condition change, and compute the performance indices using Eqs. (4.1)–(4.4).
4. Compute ΔJ_{sys} using Eq. (4.5), and rank the system cases.

The principle of decision tree classification is described separately in the following section.

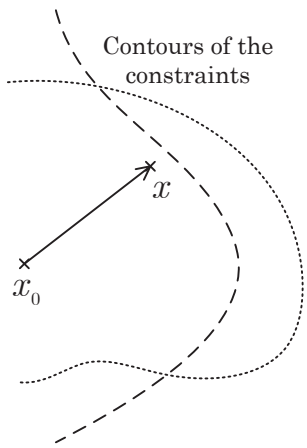

Figure 20: Projection of the system operating point.

4.4 Decision Tree Classification

The principle of a classification method is to learn through a given set of records, i.e. training data, find the model for the class as a function of other attributes, and assign a class as accurately as possible with the new unseen records. The concept of a classification method is illustrated in Figure 21. The classification task can be found in a number of applications, e.g. predicting tumor cells as benign or malignant, classifying credit card transaction, categorizing news, and etc. There are currently several classification methods:

1. Decision tree
2. Case-based reasoning
3. Artificial neural network
4. Support vector machine.

Decision tree is one of the classification methods in a form of a tree structure or tree graph, usually used for data mining and machine learning. As shown in Figure 22, there are three types of nodes in the tree:

1. Root node
2. Decision node
3. Leaf node.

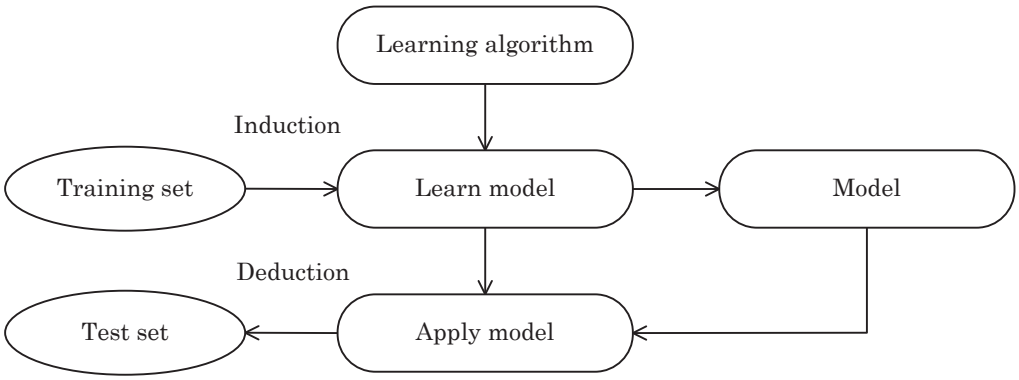

Figure 21: Classification method.

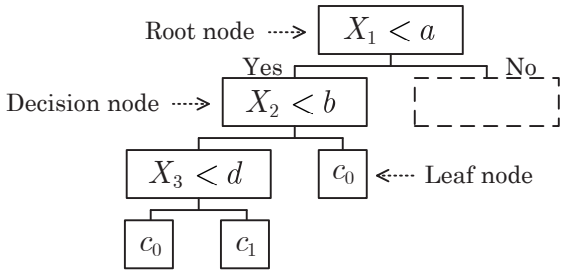

Figure 22: Example of a decision tree.

A root node is the node at the top of the tree where the classification starts. A decision node conducts a test or question, where the cases are separated, i.e. splitting a node. A leaf node provides the output classification. A decision tree classifies the case as the case is moving down the tree passing through a series of tests until it falls to one of the leaf nodes from which the class is determined. In Figure 22, $X = \{X_1, X_2, ..., X_n\}$ is a set of n input attributes and $c = \{c_0, c_1\}$ is a set of two output classes. Several applications of decision tree to the power system have been reported [35]–[38]. It is mostly used as a prediction tool for a fast system security assessment, i.e. an online transient stability assessment. In [38], the input attributes to the decision tree are obtained from phasor measurement units (PMU's). The decision tree can assess and classify whether the system status is secure or not, fast enough to allow the system operators to be prompt for proper actions.

4.4.1 Growing Algorithm

This section describes one of the well-known algorithms for growing a decision tree, i.e. CART. A decision tree is grown from the training data, similar to a neural network. The tree will represent the hidden relationship between the input attributes and output classes. Growing a decision tree is simply splitting a node based on a splitting rule.

To determine the split, we need to specify the splitting rule, i.e. a test or question. The question basically depends on the attribute types, i.e. categorical or continuous type. This section focuses on the continuous type which is relatively more difficult to deal with than the categorical type. The question for a continuous attribute is to find the threshold value. The threshold value can be determined from the location of the sorted attribute values where two adjacent classes are different. There can be a number of possible threshold values for a given attribute. In addition, there can be a number of possible splitting rules at each node to be split. The next task is to determine the best splitting rule. A good splitting rule should result in a pure separation or homogeneous class distribution. The impurity of the node; hence, the split is measured by the GINI diversity index (CART) [39]. The GINI diversity index at a

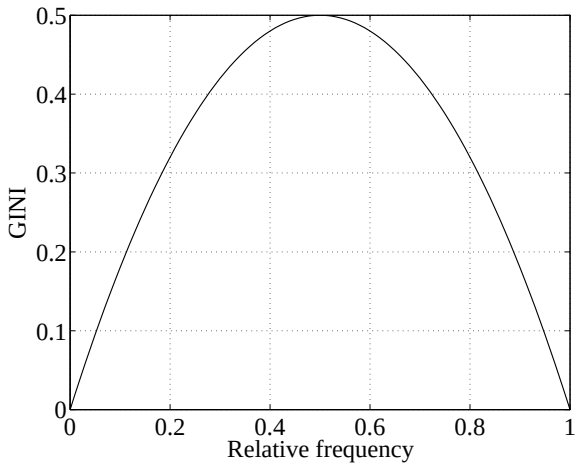

Figure 23: GINI diversity index.

given node i for a 2-class problem can be computed from

$$GINI(i) = 1 - \sum_j p(i|j)^2. \tag{4.6}$$

The maximum GINI diversity index is 0.5 when all records are equally distributed among two classes, and the minimum is zero when all records belong to one class. The comparative plot of the entropy and GINI diversity index for a 2-class problem is depicted in Figure 23. As previously mentioned, the GINI diversity index is used to measure the impurity of the split so that the best splitting rule can be determined. When a parent node p is split into two child nodes, c_1, and c_2, the quality of the split is computed from

$$GINI_{\text{split}} = \sum_{c=1}^{2} \frac{N_c}{N_p} GINI(c) \tag{4.7}$$

where N_p, N_c are the numbers of records in the parent and child nodes respectively. Therefore, the best split is the one having the minimum GINI diversity index.

The nodes are split until they are either pure, i.e. all the records in the node belong to the same class, or with the number of records smaller than the specified value, i.e. a minimum split criterion. This criterion is applied so as to avoid the over-fitting problem. The final step is to validate the obtained decision tree by testing with the test set to check its generalization.

4.4.2 Decision Tree Growing Example

To help understand the decision tree growing algorithm, a simple example is given in this subsection. In this example, a decision tree is grown by means of a recursive binary splitting

Table 3: Training set

Input attributes				Output classes
Home owner	Marital status	Annual income [$]	Split position	Loan
No	Married	60000		No
No	Single	70000		No
No	Married	75000	80000	No
No	Single	85000		Yes
No	Single	90000		Yes
No	Single	95000	97500	Yes
No	Married	100000		No
Yes	Married	120000		No
Yes	Single	125000		No
Yes	Single	220000		No

using a GINI diversity index as the impurity measure. The problem is to classify the records of the bank customers whether they apply for a loan. The input attributes and output classes are given in Table 3. There are three input attributes; two are of a categorical type, and the other is of a continuous type. There are only two output classes, i.e. "Yes" and "No" respectively.

Starting with the "Home owner" attribute as a parent node with 10 records; 3 records belong to the category "Yes" and the other 7 belong to the category "No", the node is then split to two child nodes, N_1, N_2 as depicted in Figure 24. Shown below is the calculation associated with the split. The resulting GINI diversity index of the split is found to be 0.3429.

$GINI(N_1) = 1 - \left(\frac{0}{3}\right)^2 - \left(\frac{3}{3}\right)^2 = 0$

$GINI(N_2) = 1 - \left(\frac{3}{7}\right)^2 - \left(\frac{4}{7}\right)^2 = 0.4898$

$GINI_{\text{split}} = \left(\frac{3}{10}\right)(0) + \left(\frac{7}{10}\right)(0.4898) = 0.3429$

Similarly, for the "Marital status" attribute with 10 records; 6 records belong to the category "Single" and the other 4 belong to the category "Married", the node is then split to two child nodes as depicted in Figure 24. Shown below is the calculation associated with the split. The resulting GINI diversity index of the split is found to be 0.3000.

$GINI(N_1) = 1 - \left(\frac{3}{6}\right)^2 - \left(\frac{3}{6}\right)^2 = 0.5$

$GINI(N_2) = 1 - \left(\frac{0}{4}\right)^2 - \left(\frac{4}{4}\right)^2 = 0$

$GINI_{\text{split}} = \left(\frac{6}{10}\right)(0.5) + \left(\frac{4}{10}\right)(0) = 0.3000$

Finally, for the "Annual income" attribute with 10 records. This attribute is of a continuous type; therefore, we need to find the threshold value for the split. First, the attribute values are sorted. The threshold value, i.e. split position, is determined from the mid-point where two adjacent output classes are different as shown in Table 3.

There are two possible threshold values, i.e. the annual income of $80000 and $97500 respectively. The GINI diversity index values for both split positions are computed as follows:

$GINI_{\text{split}} = \left(\frac{3}{10}\right)(0) + \left(\frac{7}{10}\right)(0.4898) = 0.3429$ for $80000 threshold

$GINI_{\text{split}} = \left(\frac{6}{10}\right)(0.5) + \left(\frac{4}{10}\right)(0) = 0.3000$ for $97500 threshold.

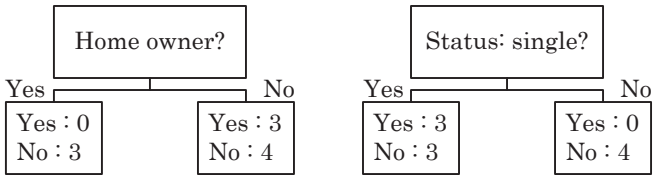

Figure 24: Illustration of the split.

Table 4: Records for the second split

Input attributes				Output classes
Home owner	Marital status	Annual income [$]	Split position	Loan
No	Single	70000	77500	No
No	Single	85000		Yes
No	Single	90000		Yes
No	Single	95000	110000	Yes
Yes	Single	125000		No
Yes	Single	220000		No

It can be seen that the $97500 threshold has smaller GINI diversity index; hence, it is selected to be the splitting rule for this attribute.

Among the GINI diversity index values of the three input attributes, those of the "Marital status" and "Annual income" attributes are the minimum of 0.3000. As a result, we can select either one of them to be the splitting rule for the first split; hence, let's select the "Marital status" attribute. The split results in two child nodes; one is pure, i.e. all records belong to the same class, but the other is not. Next we will further split the impure child node using the same procedures. The number of records is now reduced from 10 to 6 as tabulated in Table 4.

The GINI diversity index of the split for the "Home owner" and "Annual income" attributes is computed. The split positions for the "Annual income" attribute are shown in Table 4. The results are as follows:

"Home owner" attribute

$GINI_{\text{split}} = \left(\frac{2}{6}\right)(0) + \left(\frac{4}{6}\right)(0.3750) = 0.2500$

"Annual income" attribute

$GINI_{\text{split}} = \left(\frac{1}{6}\right)(0) + \left(\frac{5}{6}\right)(0.4800) = 0.4000$ for $77500 threshold

$GINI_{\text{split}} = \left(\frac{4}{6}\right)(0.3750) + \left(\frac{2}{6}\right)(0) = 0.2500$ for $110000 threshold.

The $110000 threshold has smaller GINI diversity index; hence, it is selected to be the splitting rule for this attribute.

The minimum value of the GINI diversity index of the split is 0.2500 obtained by using either one of the two attributes above for the splitting rule, here let the "Home owner" attribute

Table 5: Records for the third split

Input attributes				Output classes
Home owner	Marital status	Annual income [$]	Split position	Loan
No	Single	70000	77500	No
No	Single	85000		Yes
No	Single	90000		Yes
No	Single	95000		Yes

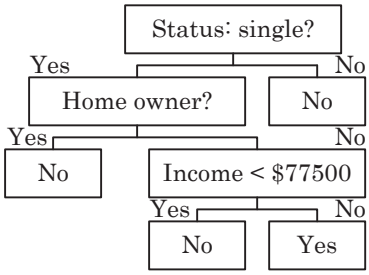

Figure 25: Resulting decision tree.

be the splitting rule for the second split. Again, the second split results in two child nodes; one is pure, but the other is not. Next, we will further split the impure child node using the same procedures. The number of records is now reduced from 6 to 4 as tabulated in Table 5.

It can be seen from Table 5 that, at this point, only the "Annual income" attribute can be used for the splitting rule because all the records of the "Marital status" attribute have the same attribute value, i.e. here same category. Furthermore, there is only one split position at $77500 as shown in Table 5, and its GINI diversity index is found to be

$GINI_{\text{split}} = \left(\frac{1}{4}\right)(0) + \left(\frac{3}{4}\right)(0) = 0.$

Finally, the resulting decision tree for this example is depicted in Figure 25.

4.4.3 Decision Tree for Transient Stability Prediction

This subsection describes a decision tree for transient stability prediction. To construct a decision tree, first we need to select the input attributes. In general, for transient stability prediction, the input attributes are commonly selected from the system parameters, e.g. bus voltage, line current, or power flow on a specific path, which can be obtained from the measurement. Basically the selected input attributes should well represent the system behavior under the transient period. In addition, the selection of the input attributes also depends on the applications, i.e. online or offline. For online applications, the attributes are usually the

available measurements, e.g. those measured by the PMU's. In contrast, for offline applications, instead of raw measurement data, data with some manipulation can also be used for the input attributes in order to obtain more accurate prediction.

In this research, a decision tree is used for system case partitioning, i.e. Filter 2 and for transient stability assessment. The input attribute of the decision tree for Filter 2 is only the shortest distance in per unit from the fault location to each generator determined from Dijkstra's algorithm [40]. Note that using only one input attribute may not yield accurate prediction but sufficient in roughly indentifying the risk-related cases due to the transient stability constraint. When applied to the system case partitoning as Filter 2, for each outage case in the Monte Carlo sample set, the vector of the value of the input attribute (i.e. the shortest fault distance to the generators) is passed through a series of questions (i.e. decision nodes) in the decision tree until falling into one of the leaf nodes which indicates whether this case is stable or not. The system cases predicted by the decision tree as unstable are regarded as severe; hence, risk-related.

On the other hand, the input attributes of the decision tree for transient stability assessment are as follows:

1. $|\Delta\delta_G|$: the absolute change in degree of a generator's rotor angle with respect to COI at pre-fault and at 5 time steps after the fault removal

2. $|\Delta\omega_G|$: the absolute change in rad/sec of a generator's rotor speed at pre-fault and 5 time steps after the fault removal

3. $|\Delta s_W|$: the absolute change in percent of a wind power induction generator's rotor slip at pre-fault and 5 time steps after the fault removal

4. d_G: the shortest impedance in per unit from the fault location to each generator determined from the Dijkstra's algorithm.

Several input attributes are added in order to attain more accurate prediction. Note that obtaining some of the input attributes requires the time-domain simulation to be performed until 5 time-steps after the fault removal as depicted in Figure 26. In Figure 26, T_0 is the first sampling time for the pre-fault state; T_1 is the fault clearing time; T_2 is the second sampling time for the post-fault state, i.e. 5 time-steps after removing the fault.

The output classes are stable (S) and unstable (U) classes. Also note that the leaf node in the decision tree can be impure, i.e. having a mix between two classes, due to the splitting criterion as mentioned previously. For Filter 2, the output class of the impure leaf node is determined from the majority. In contrast, for transient stability assessment, if the case falls into the impure leaf node, the system stability cannot be directly assessed by a decision tree; in this case, it is assessed by the time-domain simulation. The algorithm of transient stability assessment using a decision tree is summarized in Figure 27.

Since a decision tree is usually grown offline, we can use the training data as many as desired. In general, the number of cases should be large enough to cover a variety of possible

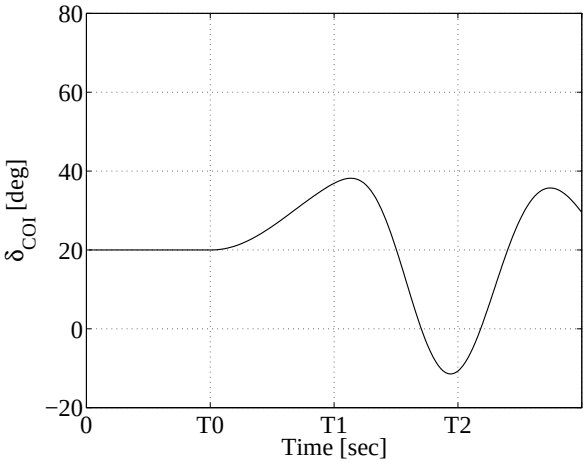

Figure 26: Sampling for the decision tree attributes.

operating conditions which may occur during an actual operation. This also basically depends on the complexity of a system under consideration. Using too few training data may result in a significant number of misclassified cases; hence, poor accuracy. These training data can be obtained either from the historical operating records if available, or by generating a number of system operating conditions, i.e. varying the demand, wind power output, and fault location.

Since the system stability can be quickly predicted by the decision tree, a significant amount of the run time can be saved. Nonetheless, the performance of the decision tree should be evaluated from time to time in order to maintain the accuracy. This can be accomplished by updating a decision tree periodically with the emerging unseen cases during the actual operation.

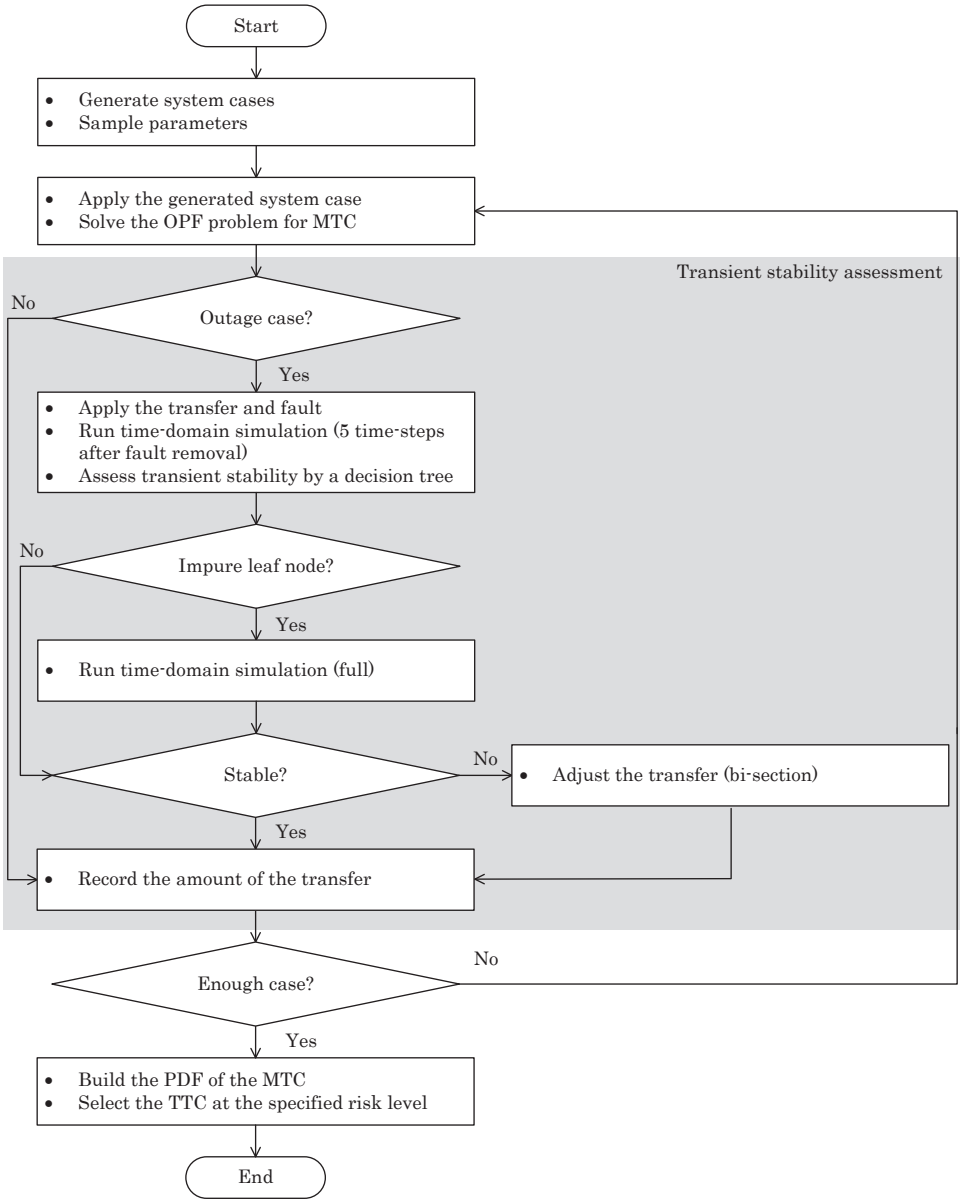

Figure 27: Probabilistic TTC evaluation with decision tree classification.

Chapter 5

Numerical Examples and Results

5.1 Results of Probabilistic Risk-Based TTC Evaluation

This section presents numerical examples, results, and discussion of the proposed TTC evaluation described in Chapter 2. There are several points to be examined, namely the impact of the uncertainty introduced by the presence of renewable energy, and that related to voltage and transient stabilities.

5.1.1 Study System

The modified IEEE 30-bus test system is used for the simulation. The system demand is increased with the total of 312.18 MW. To manifest the impact of voltage stability, the generation capacity at the source bus is increased to 400 MW. The reactive power capacities of all generators and transmission line thermal limits are also increased. More detailed descriptions on the system data are provided in the appendix. The transfer capability from bus#1 (source) to bus#12 (sink) is evaluated. In addition, it is assumed that a 125 MVAr compensator is installed at the sink bus for the voltage and reactive power support. These modifications allow the system to transfer a large amount of power; hence, operated close to the voltage stability limit. As a result, the impact of the voltage stability can be observed.

To examine the impact of the renewable energy penetration level on the TTC, 4 renewable energy penetration levels are studied as summarized in the following.

[Level 1] Original system without renewable energy

[Level 2] The system is modified by adding one 10-MW wind farm at bus#11, and one 10-MW PV system at bus#17. The total renewable energy capacity is 20 MW.

[Level 3] The system is modified by adding two 10-MW wind farms at bus#7, 11, and two 10-MW PV systems at bus#17, 18. The total renewable energy capacity is 40 MW.

[Level 4] The system is modified by adding three 10-MW wind farms at bus#7, 8, 11, and three 10-MW PV systems at bus#17, 18, 19. The total renewable energy capacity is 60 MW.

5.1.2 Parameter Set-Up

This subsection summarizes the parameter set-up for the simulation. The contingencies considered in this simulation example are those concerning outages on the transmission facilities, i.e. transmission lines and transformers up to N-2 contingencies. The probability of failure of

Table 6: Time-domain simulation parameter set-up

Time-domain simulation parameter	Setting value
Simulation time [sec]	6.00
Time step [sec]	0.01
Fault clearing time [sec]	0.35
Maximum allowable rotor angle deviation from COI [deg]	100
Maximum allowable rotor slip [%]	5

Table 7: Summary of study cases

Case	σ_{PD} [%]	σ_{PW} [%]	σ_{PV} [%]
1	-	-	-
2	10	-	-
3	10	20	20

all transmission facilities is assumed to be 0.01. The probability of a fault location is adopted from [21] as listed in Table 1 in Chapter 2. The parameter set-up for the time-domain simulation is tabulated in Table 6.

The number of samples for Monte Carlo simulation is 5000 which is found to be sufficient for the convergence of the simulation process. The convergence of the simulation process is indicated by the convergence of the mean MTC. The simulation results will be presented and discussed in detail in the following subsections.

5.1.3 Impact of Uncertainty

Several points regarding the impact of the uncertainty on the TTC are examined as we move along this subsection. First, we investigate the impact of the uncertainty degree and observe how the TTC behaves as the uncertainty degree increases. Level 4 is used for the investigation with three comparative study cases given in Table 7. Here voltage and transient stabilities are not considered.

In Table 7, $\sigma_{PD}, \sigma_{PW}, \sigma_{PV}$ are the standard deviations of the forecast demand, wind power output, and PV output respectively. They are specified in percent of the forecast value as mentioned in Chapter 2. In brief, Case 1 is without any uncertainty except that of equipment availability, i.e. setting all standard deviations to zero. Case 2 introduces the uncertainty of the forecast demand. Case 3 introduces the uncertainty of both forecast demand and forecast renewable energy power outputs.

Figure 28 shows the convergence of the mean MTC for the given 5000 sample cases. The PDF's of the MTC for all three study cases are depicted in Figures 29–31. The TTC values are tabulated in Table 8.

Table 8: Summary of the TTC values

Risk	TTC [MW]		
[%]	Case 1	Case 2	Case 3
5	217.91	218.69	218.15
10	232.46	231.67	231.46
15	240.53	237.04	236.51
20	244.83	239.98	239.59

The simulation results show that in general for most risk levels except at 5%, the TTC gradually decreases due to the presence of the uncertainty. This can be simply explained from the PDF of the MTC. The uncertainty generally causes the shape of the PDF to change and become more scattering, i.e. the MTC values redistribute. Most MTC's lying at around 248.57 MW in Case 1, scatter due to the change in the operating point from which the MTC is computed. These redistributing MTC's result in the probability density distribution at the smaller transfer amount; as a result, the TTC at risk decreases. For instance, consider the TTC at 15%, in Case 2, the forecast demand uncertainty results in the scattering PDF and the TTC slightly decreasing from 240.53 MW in Case 1 to 237.04 MW. Finally, the PDF of Case 3 has the most scattering shape since the uncertainty of all forecast parameters is included. This also results in the smallest TTC of 236.51 MW.

Furthermore, the monetary loss can also be used to evaluate the impact of the uncertainty. According to the risk concept described in Chapter 2, the risk occurs when the maximum transferable power is smaller than the specified TTC. This circumstance results in interrupted energy to end-users. The monetary impact from the interruption can be described by the risk function expressed as follows:

$$R(x) = \sum_{x=0}^{TTC} IEAR(TTC - x)p(x) \tag{5.1}$$

where $IEAR$ is an interrupted energy assessment rate (in \$/MWh) [41]; x is the MTC; $p(x)$ is the probability of x.

Suppose that the system operator simply neglects the uncertainty and given the $IEAR$ of 500\$/MWh. The TTC at 15% risk will be set to 240.53 MW (Case 1) with the expected monetary loss of 1577\$/hr. Nonetheless, due to the PDF shift, the actual risk and monetary loss become 21.9% and 1809\$/hr, both higher than expected. This is analogous to moving the dashed line in Figure 31 slightly to the right. Therefore, it is clear that neglecting the uncertainty leads to an optimistic TTC which is impractical and not secure.

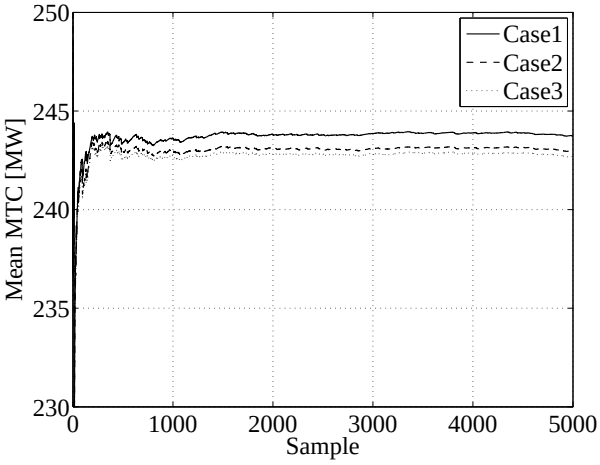

Figure 28: Convergence of the mean MTC.

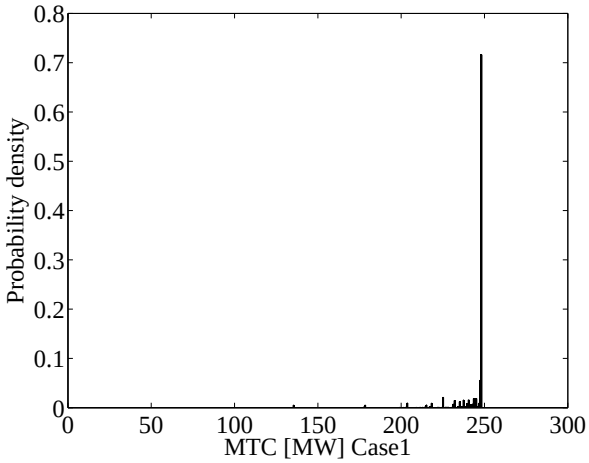

Figure 29: PDF of the MTC (Case 1).

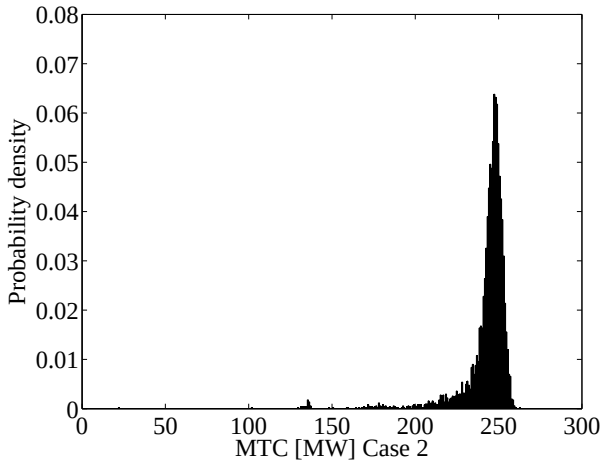

Figure 30: PDF of the MTC (Case 2).

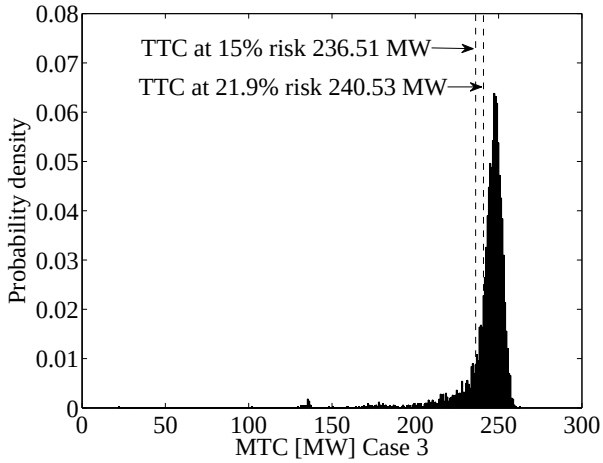

Figure 31: PDF of the MTC (Case 3).

Table 9: Summary of the TTC values for 4 penetration levels

Risk [%]	TTC [MW]			
	Level 1	Level 2	Level 3	Level 4
5	198.61	204.80	213.05	218.15
10	214.42	219.92	226.01	231.46
15	219.37	224.47	230.26	236.51
20	220.07	227.29	233.10	239.59

Table 10: Summary of study cases

Case	Voltage stability assessment	Transient stability assessment
1	No	No
2	Yes	No
3	Yes	Yes

The next point to be examined is how the TTC changes as the renewable energy penetration level increases from Level 1 to Level 4. The resulting TTC values are tabulated in Table 9. It is expected that the impact of the uncertainty will become noticeable at the high penetration level. This is because of the increase in the parameters subjected to the uncertainty. Although the uncertainty from renewable energy causes the TTC to drop, the obtained results show that, in overall, the TTC still increases. This is due to the fact that the presence of the renewable energy assists in supplying the demand located nearby; as a result, alleviating the transmission line loading, the voltage drop, i.e. allowing more transfer. Besides, the source generator has more capacity left for conducting the transfer. These two factors cancel out each other while yielding a gradually increasing TTC.

5.1.4 Impact of Voltage and Transient Stability Constraints

In addition to the uncertainty previously investigated, we also examined the impact of both voltage and transient stability constraints. Here the voltage stability margin is set to 35%. The threshold value is set to 0.27 which is determined from the preliminary study with another set of system conditions similar to those used in the TTC evaluation. From the security point of view, the threshold value should be selected such that it covers all the cases having the voltage stability margin less than the specified value. Setting the threshold value too large can lead to some cases missed during the assessment. On the other hand, setting the threshold value too small may result in a number of cases to be assessed; hence, time-consuming. To examine the impact of the voltage and transient stabilities on the TTC, three comparative study cases are conducted as listed in Table 10. The simulation is conducted on Level 4.

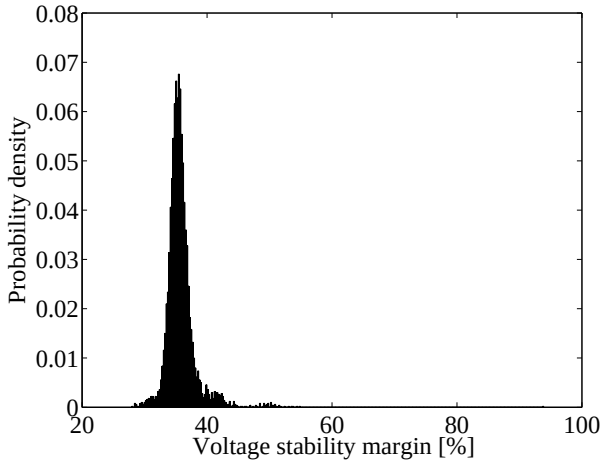

Figure 32: PDF of the voltage stability margin.

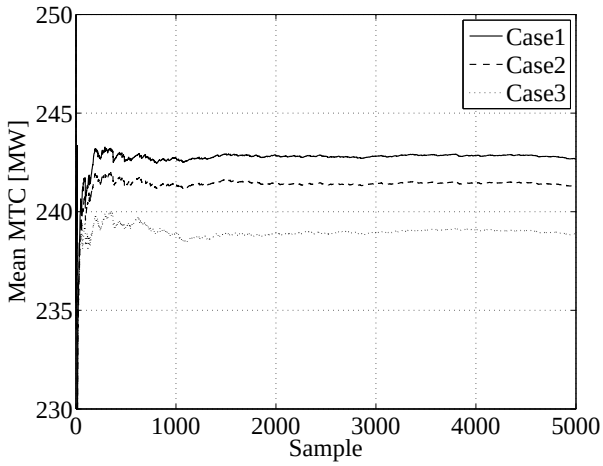

Figure 33: Mean MTC.

Table 11: Summary of the TTC values

Risk	TTC [MW]		
[%]	Case 1	Case 2	Case 3
5	218.15	217.79	199.73
10	231.46	228.82	219.41
15	236.51	233.76	228.92
20	239.59	238.08	234.32

First, for verification, the voltage stability margin in percent of all 5000 cases is computed using Eq. (5.2), and its probability density function, PDF is shown in Figure 32.

$$\text{Margin} = \frac{P_{\text{nose}} - MTC}{P_{\text{nose}}} \times 100. \tag{5.2}$$

Here P_{nose} is the maximum loadable power at the nose-point. The margin ranges from 27.91% to 93.90% with the average of 35.81%. It is found that out of the 5000 cases, 1784 cases have the voltage stability margin less than the specified 35%. As a result, the transfer amounts of these cases are reduced by the voltage stability assessment. The minimum voltage stability index within a set of the cases having insufficient margin is 0.2764. Therefore, using the specified threshold still covers all of them. Larger threshold values can also be used to further speed up the computation but it may degrade the accuracy. Furthermore, some cases skipped due to a large threshold setting may encounter transient instability; hence, requiring more run time for the transient stability asssessment (i.e. the overall computational speed is not improved).

The transfer reduction causes the mean MTC to drop from 242.67 MW (Case 1) to 241.30 MW (Case 2). Interestingly, this reduction can be clearly seen from the shape of the PDF of the MTC that the right part of the PDF in Case 2 shifts to the left. Further, when considering the transient stability constraint, the mean MTC further drops from 241.30 MW (Case 2) to 238.84 MW (Case 3). This is also due to the fact that the transfer amounts of the 425 unstable cases are reduced by the transient stability assessment. For this numerical example, the total amount of the transfer reduced due to the voltage stability constraint is 6860.8 MW and that due to the transient stability constraint is 12298.0 MW respectively.

Next consider the risk-based TTC values selected at 4 different risk levels as tabulated in Table 11. The results show that, similar to the mean MTC, the TTC also drops from Case 1 to Case 3. To give an example, the TTC selected at 15% risk drops from 236.51 MW (Case 1) to 233.76 MW (Case2), and to 228.92 MW (Case 3).

Interestingly, unlike the mean MTC, the TTC strongly depends on the shape of the PDF from which it is selected. The TTC drop in Cases 2 and 3 results from the PDF shift as shown in Figures 37 and 38. They depict the PDF's of the MTC before and after their transfer amounts are reduced by the voltage and transient stability assessment respectively. As seen from Figure 37, the PDF shift due to the voltage stability constraint mostly occurs in the MTC range above 230 MW; hence, this causes the TTC selected at high risk levels, i.e. beyond

10% to drop. In contrast, the PDF shift due to the transient stability constraint as shown in Figure 38 mostly occurs in the lower MTC range. Therefore, the drop in the TTC can also be seen even at the low risk levels.

Also note from the results that the drop in the TTC due to the transient stability constraint is eminent at low risk levels. This is because it takes several bins in the low MTC range to make up for the probability of the cases having the MTC reduced due to the transient instability. To give an example, in this numerical example, there are a total of 425 unstable cases accounting for about 0.085 probability. This probability shifts to the lower MTC range in the PDF. The PDF here is simply a histogram composing of a number of bins storing the MTC values. When the risk level is low, i.e. at 5%, the location of the TTC is in the MTC range, where each bin contains only a small portion of the probability, i.e. a small number of cases in each bin. As a result, the TTC drops significantly since many bins are required to make up for the 0.085 probability of the unstable cases. On the other hand, when the risk level is high, the location of the TTC moves further to the right of the PDF, where each bin contains a large portion of the probability, i.e. a large number of cases in each bin. As a result, the 0.085 probability of the unstable cases can be easily made up by only one or a few bins, resulting in less apparent drop in the TTC.

The voltage and transient stabilities can be a serious problem for some particular systems, where a special attention is required to ensure the system security. Therefore, it would be better to always implement the proposed voltage and transient stability assessment during the TTC evaluation to make sure that we will not overlook such circumstances.

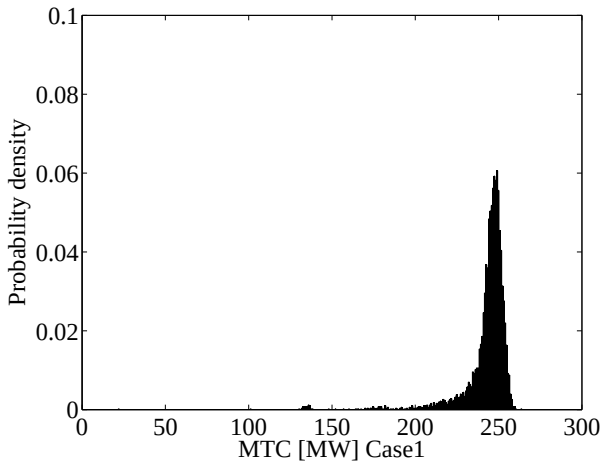

Figure 34: PDF of the MTC (Case 1).

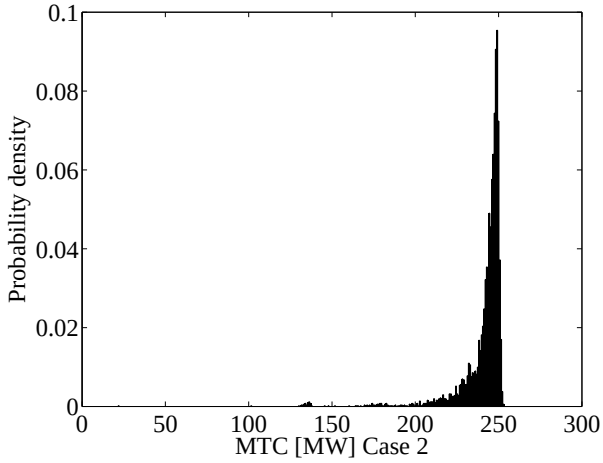

Figure 35: PDF of the MTC (Case 2).

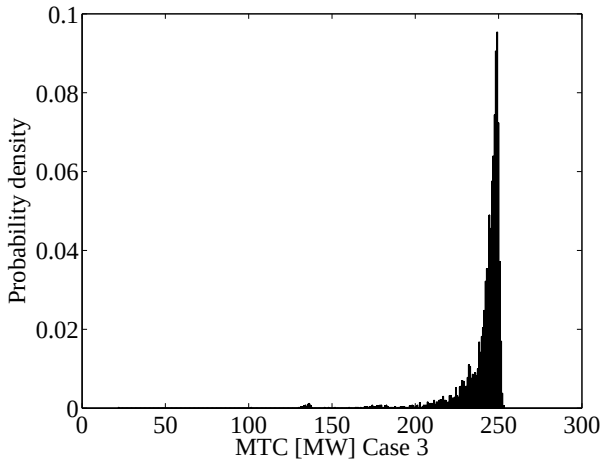

Figure 36: PDF of the MTC (Case 3).

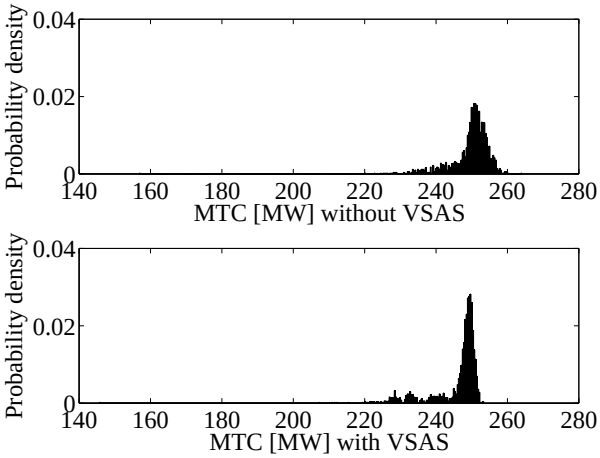

Figure 37: PDF shift due to the voltage stability constraint.

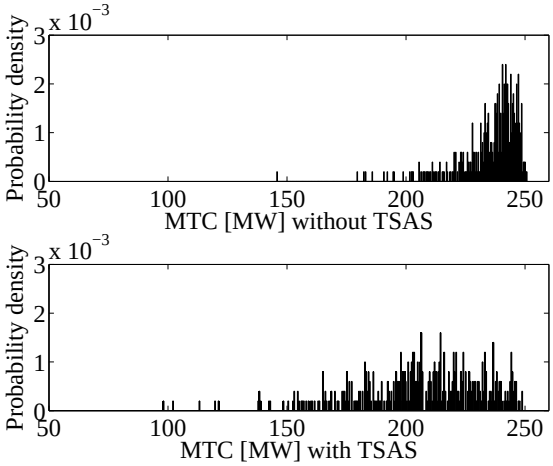

Figure 38: PDF shift due to the transient stability constraint.

5.2 Results of Efficient TTC Evaluation

5.2.1 Study System

This section investigates the efficiency of the proposed efficient TTC evaluation method described in Chapter 4, through a numerical simulation conducted on the modified IEEE 30-bus system with a single-line diagram shown in Figure 39. The system has 6 conventional thermal power plants with the total capacity of 355 MW and with the total demand of 208.12 MW. Three 10 MW wind farms are added at buses#7, 8, and 11. Three 10 MW PV systems are added at bus#17, 18, and 19. The transfer capability from bus#1 (source) to bus#12 (sink) is evaluated. Please be cautioned that this test system is different from the one used in the previous section.

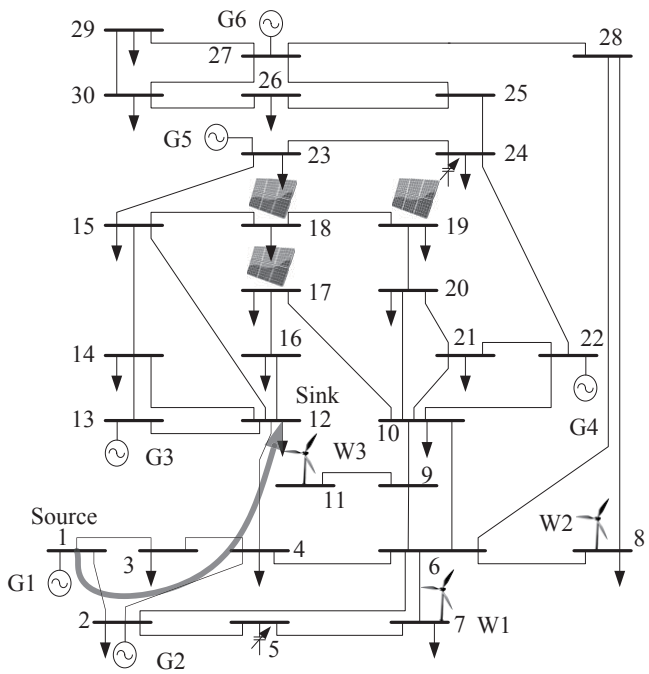

Figure 39: Modified IEEE 30-bus system with renewable energy.

Table 12: Summary of the pertitioned sets

Sub-case	Number of samples
a	1000
b	2000
c	3000
d	5000

5.2.2 Parameter Set-Up

The forecast power outputs of each wind farm and PV system are 7.5 and 8 MW respectively. The standard deviation of the forecast demand is 10% and that of the forecast renewable energy power output is 20%. The probability of a fault location and parameter set-up for time-domain simulation are the same as tabulated in Tables 1 and 6 except the maximum allowable rotor angle with respect to COI which is reduced to 80 degrees. The total number of samples for Monte Carlo simulation is 5000. The simulation is run on a Pentium Core2Duo 2.4 GHz PC with 4 GB RAM.

The decision tree is grown from the training data of 3000 samples and tested with the testing data of 1000 samples. These data sets are obtained from the system case generation used for the training data preparation. They can also be retrieved from actual historical operating records if available. The minimum split criteria are 100 and 50 respectively.

To validate and examine the performance of the proposed method, two comparative study cases are conducted as follows:

Case 1: the TTC is evaluated with the system case partitioning and transient stability is assessed by the time-domain simulation.

Case 2: the TTC is evaluated with the system case partitioning and transient stability is assessed by a decision tree.

Several partitioned sets (i.e. sub-cases) with different numbers of samples are examined as tabulated in Table 12. The performance in terms of the accuracy and computational speed enhancement will be presented and discussed.

5.2.3 Results of Case 1

In this case, the TTC is evaluated with the system case partitioning and transient stability is assessed by the time-domain simulation. Out of 2023 outage cases, there are 178 unstable cases. The decision tree for Filter 2 is shown in Figure 40. The testing error is 7.5%. The tree classifies the case by first checking whether the shortest fault distance to the generator#2 is less than 0.207. If yes, the case will move down to the next question, i.e. the second decision node on the left; otherwise, it will go to the decision node on the right. The case will pass through this series of questions until it reaches the leaf node from which the output class (i.e. either stable or unstable) is provided. The number of unstable cases classified by this decision

tree is 427 which is larger than the actual number of 178. However, the overall accuracy is not much a concern here as long as the actually unstable cases are classified correctly.

The comparison of the MTC distribution between without and with ranking are shown in Figures 41 and 42. It can be seen that the proposed system case partitioning method can successfully rank the risk-related cases. In Figure 42, the position to the left corresponds to the most severe cases whereas that to the right corresponds to the least severe cases. As a result, when the partitioned set is built by selecting the cases starting from the left to the right. These risk-related cases will be captured into the set.

The TTC values are summarized in Table 13. It is obvious from the simulation results that the more cases used, the more accurate result. The accuracy here is determined by comparing with the result of Case 1d where all 5000 samples are used. It can be observed from Table 13 that the TTC obtained by using the partitioned set with the number of samples less than 5000 is slightly larger than the actual TTC. This implies that the partitioned set does not cover all the risk-related cases. The TTC errors from Case 1d in percent, ΔTTC, are also tabulated in Table 14. The TTC errors generally reduce as more cases are included in the partitioned set. Interestingly, it can also be noted that when using a small number of samples, i.e. Case 1a, the TTC error increases with the specified risk. This is because first obtaining the TTC at high risk requires a sufficient number of samples to build the probability distribution covering the range from which the TTC is selected. Thus, the partitioned set with a small number of samples may not cover all the risk-related cases. Second, the samples required for building the distribution at high risk are composed of both severe and fairly severe system cases (i.e. having fairly large MTC). Unlike the severe system cases, it is relatively difficult to accurately rank the fairly severe system cases, i.e. the values of ΔJ_{sys} are not much different.

To achieve a given level of accuracy for TTC, the number of samples should be more than that required for building the distribution. For example, given the total number of samples of 5000, the TTC at 20% risk requires at least 1000 samples for building the distribution for the TTC selection. It can be seen from the results that using only 1000 samples cannot get the accurate TTC (i.e. with the error as much as 9.11%). In this example, it is better to use 2000 samples (Case 1b) or 3000 samples (Case 1c) which is sufficient to obtain the TTC with the error less than 1%.

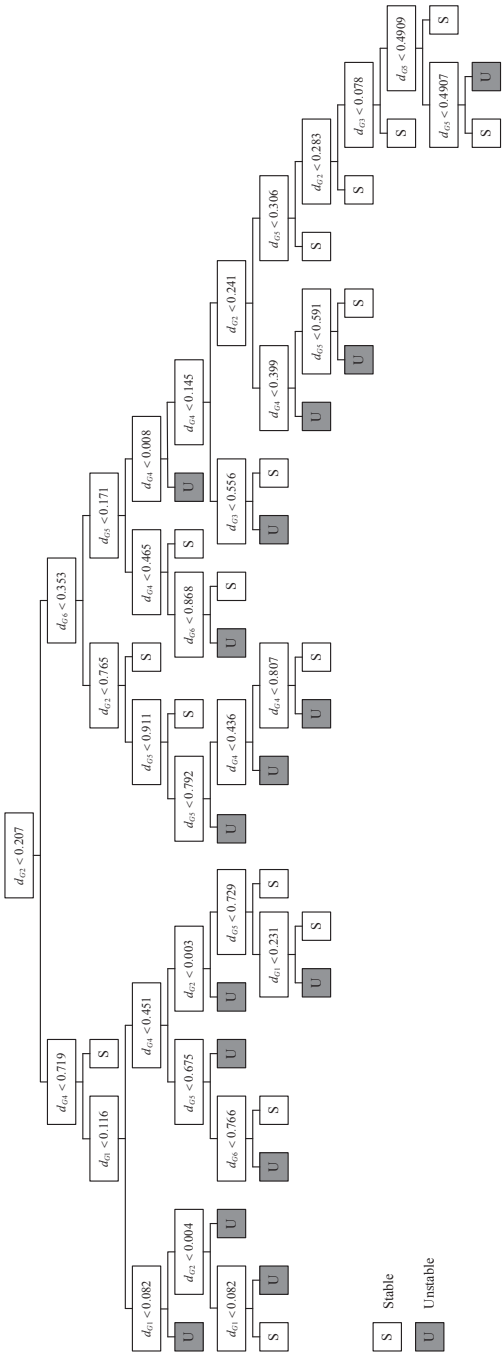

Figure 40: Decision tree for system case partitioning (Filter 2).

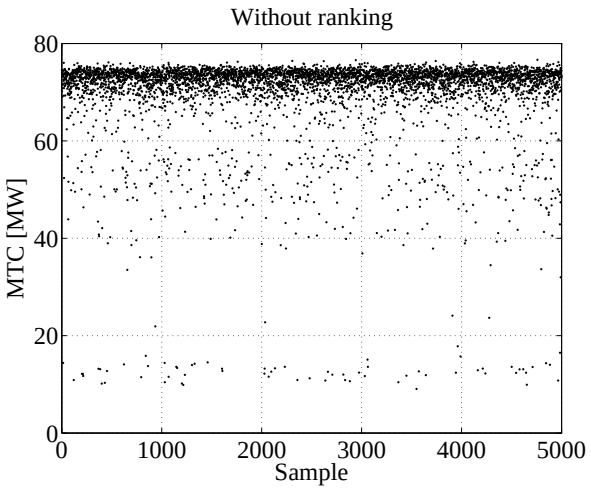

Figure 41: MTC distribution without ranking.

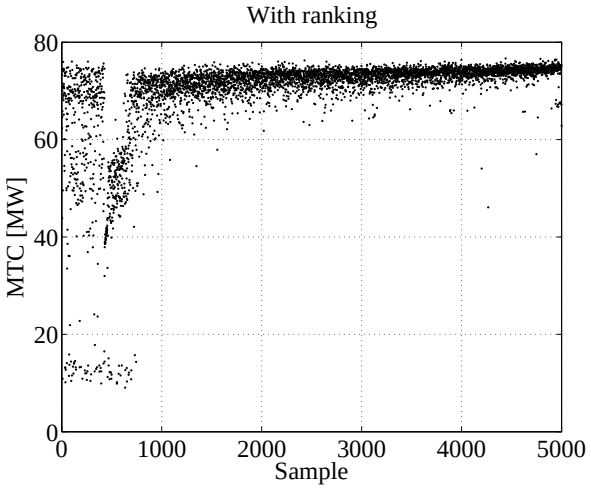

Figure 42: MTC distribution with ranking.

Table 13: Summary of the TTC values (Cases 1a–1d)

Risk	TTC [MW]			
[%]	Case 1a	Case 1b	Case 1c	Case 1d
5	51.43	51.43	51.43	51.39
10	64.93	63.63	63.57	63.46
15	70.46	68.75	68.55	68.31
20	76.02	70.24	69.87	69.67

Table 14: Summary of the ΔTTC (Cases 1a–1c)

Risk	ΔTTC [%]		
[%]	Case 1a	Case 1b	Case 1c
5	0.08	0.08	0.08
10	2.32	0.27	0.17
15	3.15	0.64	0.35
20	9.11	0.82	0.29

5.2.4 Results of Case 2

In this case, the TTC is evaluated with the system case partitioning. For transient stability assessment, instead of the full time-domain simulation, a decision tree is used to fast predict the system stability. The decision tree for transient stability assessment is shown in Figure 43. Since several input attributes are used, the size of the tree (i.e. the number of nodes) is smaller than that used for Filter 2. The testing error is 1.0%. Similar to Case 1, several partitioned sets (i.e. sub-cases) are examined.

Out of the 2023 outage cases, there are 23 stable cases misclassified as unstable and 128 cases falling into the impure leaf nodes. Therefore, in terms of the accuracy, the decision tree performs well in predicting the system stability, i.e. only 1.14% misclassified. This also infers that the selected input attributes can well represent the system behavior under the transient period. The misclassification results in the TTC errors, i.e. slightly smaller than the actual value. Here the TTC of Case 1d is used as the reference for comparison. The TTC values and errors from Case 1d in percent, ΔTTC, are also given in Tables 15 and 16. The same trends of the accuracy as found in Case 1 can also be observed in Case 2. Interestingly, given the same partitioned set and risk level, the TTC of Case 2 is sometimes more accurate than that of Case 1. This is because the errors from misranking and decision tree misclassification cancel out each other.

Table 15: Summary of the TTC values (Cases 2a–2d)

Risk	TTC [MW]			
[%]	Case 2a	Case 2b	Case 2c	Case 2d
5	50.10	51.10	51.10	51.39
10	63.53	62.95	62.93	62.77
15	70.25	68.58	68.36	67.94
20	76.02	70.18	69.81	69.58

Table 16: Summary of the ΔTTC (Cases 2a–2d)

Risk	ΔTTC [%]			
[%]	Case 2a	Case 2b	Case 2c	Case 2d
5	2.51	2.51	2.51	0.00
10	0.11	0.80	0.84	1.09
15	2.84	0.40	0.07	0.54
20	9.11	0.73	0.20	0.13

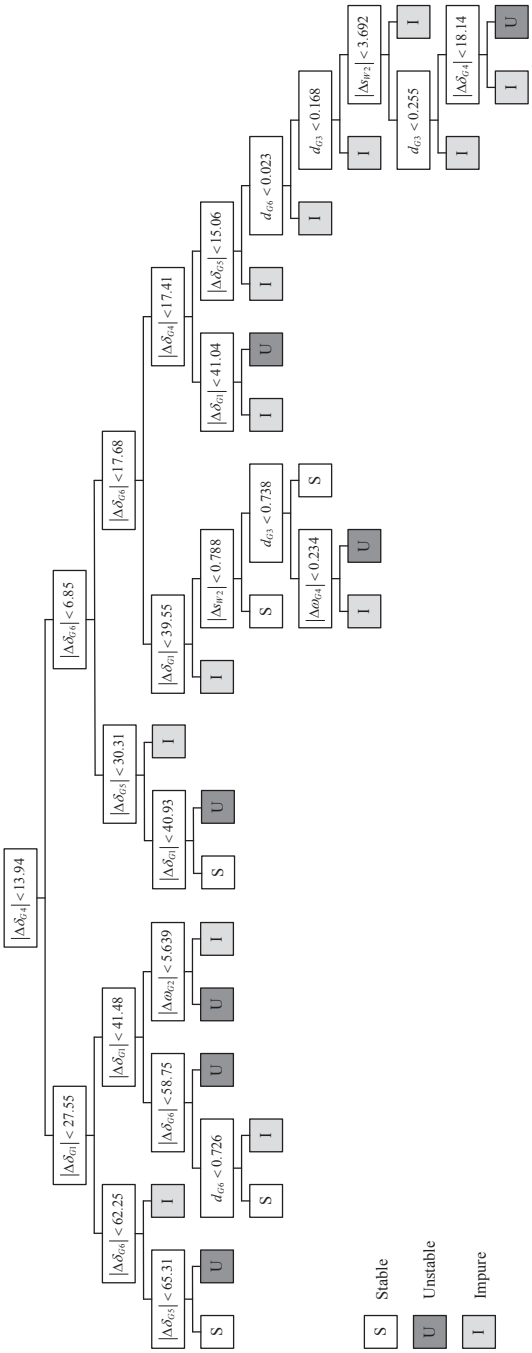

Figure 43: Decision tree for transient stability assessment.

5.2.5 Comparison of the Run Time

This subsection examines the performance in terms of the computational speed enhancement. The run time of Case 1d of 4373 sec is used as the reference for comparison. The run time of Cases 1a–1d and Cases 2a–2d is listed in Tables 17 and 18 respectively. The run time for the system case partitioning process is 50 sec. The decision tree growing takes less than 1 sec for both trees. It is obvious from the results that the run time strongly depends on the number of samples, i.e. the more samples used, the more run time required. In Case 1, the run time is saved mainly due to the reduction of the number of cases to be evaluated. In Case 2, the run time is further saved when using the decision tree for transient stability prediction. Hence, given the partitioned set with the same number of samples, the run time of Case 2 is less than that of Case 1.

The proposed method can save a significant amount of the run time. For instance, the TTC can be obtained within 1255 sec (Case 2b) accounting for only 29% of the total run time (i.e. 4373 sec) with the error less than 1%. The computational speed can be further improved if the simulation task is distributed to several PC's. Nonetheless, there is always a tradeoff between speed and accuracy, if the accuracy is the primary concern, a sufficient number of samples should be included in the partitioned set.

Table 17: Summary of the run time (Cases 1a–1d)

Case	Run time [sec]
1a	2001
1b	2717
1c	3296
1d	4373

Table 18: Summary of the run time (Cases 2a–2d)

Case	Run time [sec]
2a	1097
2b	1255
2c	1669
2d	2632

5.3 Results of TTC Evaluation with LVRT Consideration

This section examines the impact of Low Voltage Ride-Through (LVRT) consideration on the TTC. Consideration of LVRT is expected to have an impact on the transient stability since some of the wind farms or PV systems may be disconnected from the grid during the fault. This disconnection can either improve or degrade the system stability, which depends on several factors, e.g. the fault locations, system configuration, size of a wind farm or PV system, etc. What is of interest here is the impact on the TTC. Note that the TTC is evaluated here based on the probabilistic method taking into account the stochastic nature of the system and faults. Such faults which cause the disconnection of a number of generation units may not occur frequently; hence, not much impact imposed on the TTC. This aspect will be investigated through the following simulation examples.

5.3.1 Impact of LVRT on Transient Stability

This subsection shows two fault conditions which have different impacts on the transient stability, i.e. one improves but the other degrades the transient stability. Shown in Figure 44, a modified 9-bus test system with a PV system installed at bus#7 is used for the simulation. The system has 3 conventional thermal power stations with the total capacity of 820 MW and with the total demand of 315 MW. Please see the appendix for more details on the test system data. The time-domain simulation is run for 20 sec with the time step of 0.01 sec. The fault is applied with the clearing time of 0.45 sec, relatively long in order to create a severe fault condition.

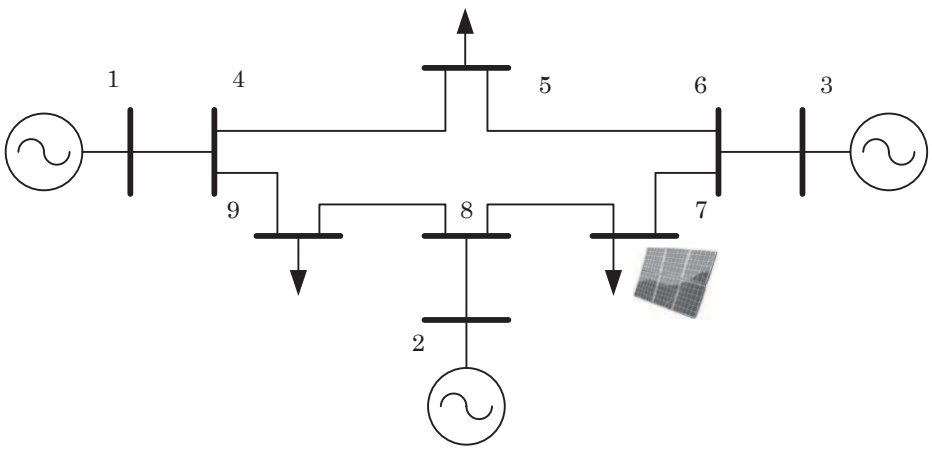

Figure 44: Modified 9-bus test system.

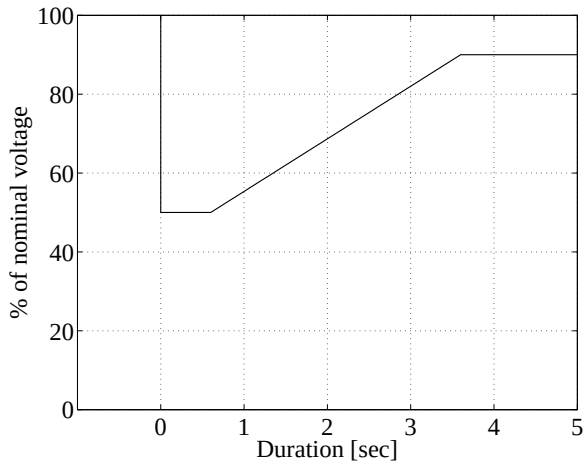

Figure 45: LVRT characteristic for the simulation.

The LVRT characteristic applied here is shown in Figure 45 with the minimum voltage of 50% of the nominal value for 0.625 sec, and recovery time of 3 sec reaching back to 90% of the nominal value. First, we will show the case where LVRT consideration improves the transient stability. The size of the PV system is 50 MW. The fault is applied on the line connecting between buses#6 and 7 near the PV system bus. Comparative plots of the generator's rotor angle with respect to the COI, generator's rotor speed (frequency), and PV system bus voltage between two cases, i.e. without tripping criterion and with LVRT, are given in Figures 46–50. Please be cautioned to note that 'without trippuing criterion' refers to the case where all generating units are assumed to be able to ride through the fault regardless of the drop in the terminal voltage. This assumption has also been adopted throughout the simulation presented in the previous sections. On the other hand, 'with LVRT' refers to the case where the LVRT characteristic curve is imposed. The generating units are required to ride through the fault as specified in the curve. The generating units which fail to comply with the curve are disconnected from the grid.

It can be seen from Figure 50 that the terminal voltage of the PV system drops below 50% shortly after the fault. As a result, the PV system is disconnected. This disconnection of 50 MW PV system is found to improve the system stability as seen from the generator's rotor angle with respect to the COI. In this simulation, generator#3 at bus#3 is apparently affected the most among all three generators since it is near the PV system. The fault first causes all generators to accelerate. Disconnection of the PV system in this case helps reduce the accelerating power during the fault which can be observed through the drop in the generator's rotor speed (i.e. frequency) as shown in Figure 49. This means that all generators are speeding up at a smaller rate. As a result, it is seen from the COI that generator#3 comes slightly closer relative to the rest.

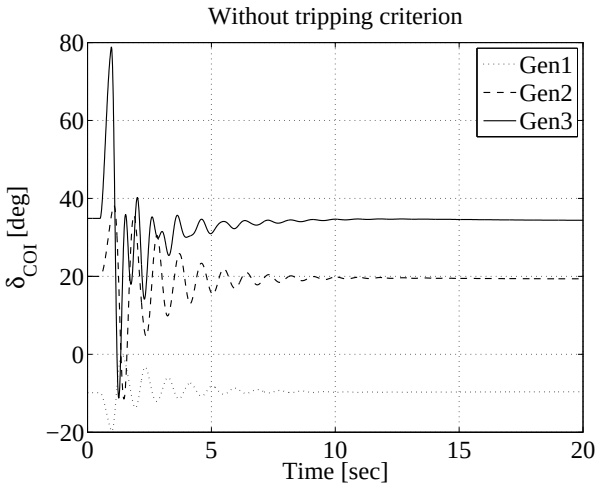

Figure 46: Rotor angle (COI) without tripping criterion.

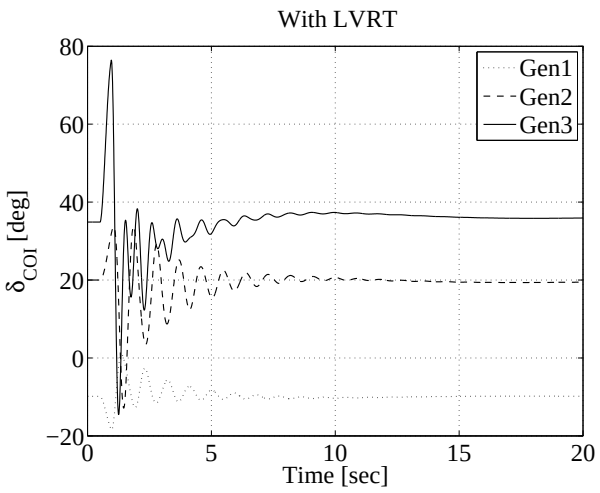

Figure 47: Rotor angle (COI) with LVRT.

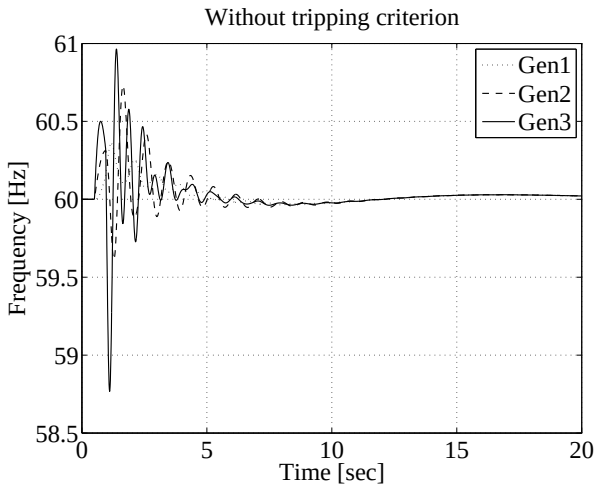

Figure 48: Frequency without tripping criterion.

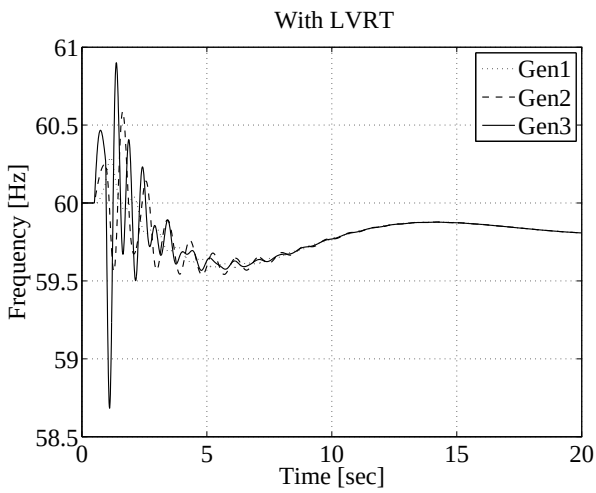

Figure 49: Frequency with LVRT.

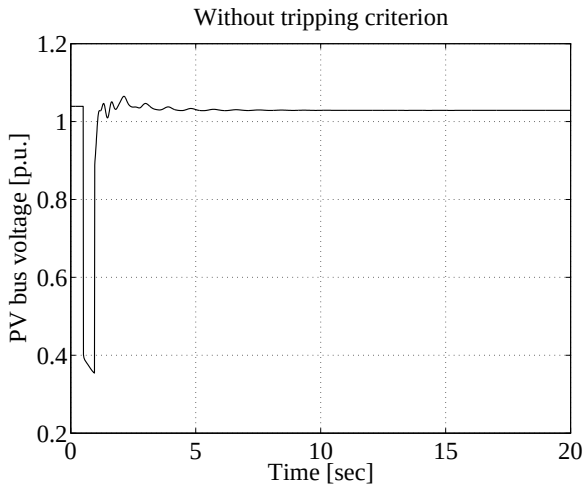

Figure 50: PV system bus voltage.

Please also note that since the transient stability analysis usually concerns only a short time interval following the disturbances, i.e. 3–10 sec, secondary responses for redispatching the generation (i.e. recovering the system frequency back to the nominal frequency) are not considered.

Next, we will show the case where LVRT consideration degrades the transient stability. The size of the PV system is 180 MW, relatively larger than the previous example. Therefore, it is expected that losing the PV system may degrade the system stability. The fault is applied on the line connecting between buses#3 and 6 also near the PV system bus. Comparative plots of the generator's rotor angle with respect to the COI, generator's rotor speed (frequency), and PV system bus voltage between without tripping criterion and with LVRT cases are given in Figures 51–55.

Similar to the previous example, the terminal voltage of the PV system drops below 50% shortly after the fault. As a result, the PV system is disconnected from the grid. Nonetheless, in this case, disconnecting a large 180 MW PV system degrades the transient stability as clearly seen from Figure 52 that the generator#3 suddenly steps out and loses synchronism with the rest. Although the accelerating power of all generators during the fault is reduced by the disconnection of the PV system, as seen from Figure 54, the frequency of the generator#3 drops at first following the disconnection of the PV system, but shortly after the fault is removed, it begins to increase again, and the generator#3 finally becomes out of step. This sudden increase in the rotor speed is as a result of the disconnection of a PV system. It is also interesting to note that since the system loses a large generating unit, the generators' frequencies drop significantly from the nominal value finally reaching 59.2 Hz after 20 sec.

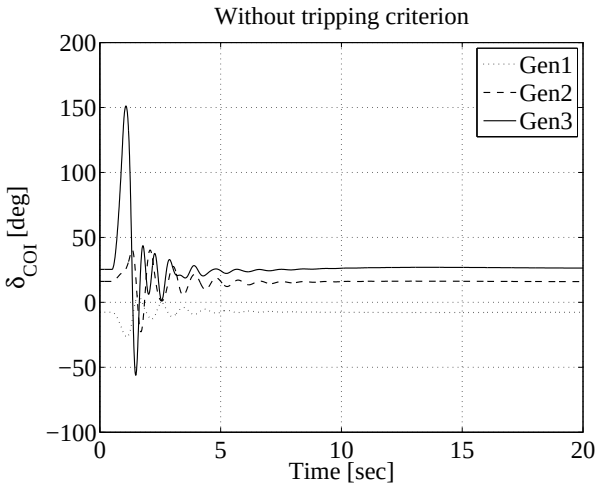

Figure 51: Rotor angle (COI) without tripping criterion.

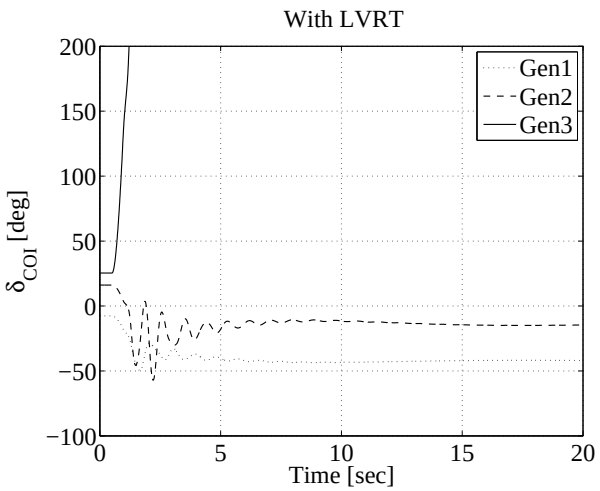

Figure 52: Rotor angle (COI) with LVRT.

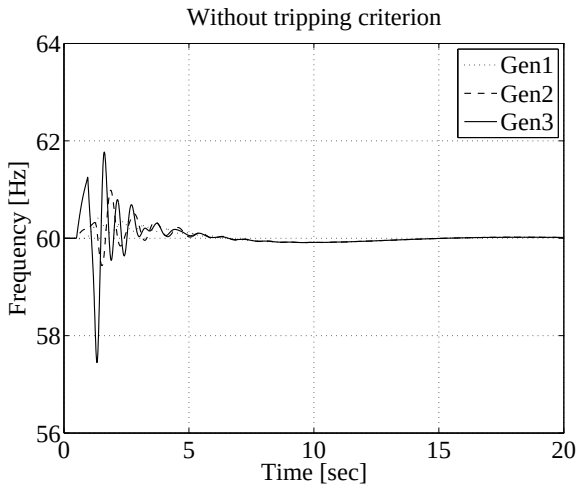

Figure 53: Frequency without tripping criterion.

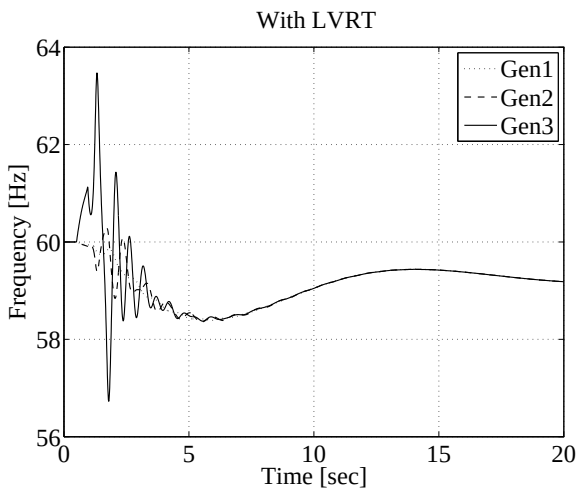

Figure 54: Frequency with LVRT.

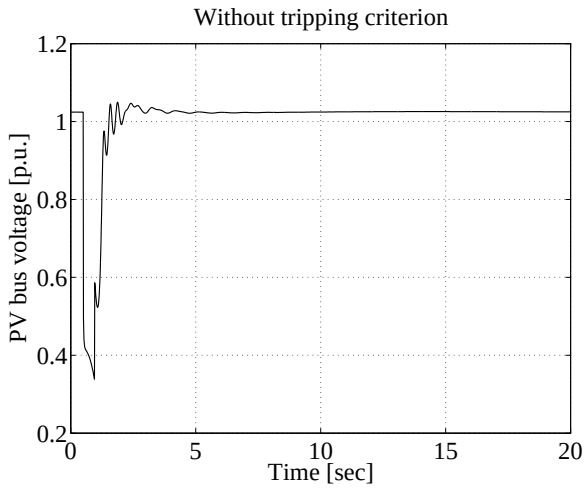

Figure 55: PV system bus voltage.

It can be concluded from the simulation results that the impact of LVRT consideration on the transient stability can be either good or bad depending on several factors. One of them which is made clear here is the size of the generating unit, i.e. a PV system, that is disconnected during the fault. Not only the size but also other related factors, e.g. system configuration, fault locations, etc contribute to the system behavior under the transient periods in a very complex way.

5.3.2 Impact of LVRT on TTC

It is known from previous subsection that LVRT consideration has an impact on the system transient stability. The faults which cause large generation units to be disconnected degrade the transient stability; however, such faults may not occur so frequently that they can pose a significant impact on the TTC. The following simulation example is to examine this aspect. To do so, three comparative study cases are conducted as follows:

Case 1: TTC evaluation without tripping criterion

Case 2: TTC evaluation with LVRT consideration

Case 3: TTC evaluation with fixed 90% voltage tripping criterion.

It should be emphasized again that 'without tripping criterion' refers to the case where all generating units are assumed to be able to ride through the fault regardless of the drop in the terminal voltage, i.e. always remaining connected to the grid. The simulation is carried out on the 9-bus system with 180 MW PV system connected at bus#7. The time-domain simulation parameter set-up is given in Table 19. The LVRT characteristic is the same as the one used in the previous subsection.

Table 19: Time-domain simulation parameter set-up

Time-domain simulation parameter	Setting value
Simulation time [sec]	6.00
Time step [sec]	0.01
Fault clearing time [sec]	0.45
Maximum allowable rotor angle deviation from COI [deg]	120

Table 20: Comparison of the TTC values

Risk	TTC [MW]			ΔTTC [MW]	
[%]	Case 1	Case 2	Case 3	Case 2	case 3
5	249.62	248.44	248.44	1.18	1.18
10	272.56	272.29	272.29	0.27	0.27
15	281.06	281.01	281.01	0.08	0.08
20	284.19	284.19	284.19	0.00	0.00

Out of 1342 outage cases, the number of unstable cases are 40, 47, and 50 for Cases 1–3 respectively. In this example, disconnection of the PV system is found to cause more cases become unstable. The comparison of the TTC values is given in Table 20. As expected, this results in a slight drop in the TTC of Cases 2 and 3 when compared to that of Case 1. Although Case 3 has more unstable cases than Case 2, the obtained TTC values are the same for the given risk levels.

It can be concluded from the simulation results that LVRT consideration does not impose much impact on the TTC. Such particular faults which cause the disconnection of large generating units usually do not occur often. In addition, the scale of the test system used in this simulation example is rather small where the generators could be easily affected by the disconnection of generating units. In case of a larger system, especially, where generating units, i.e. wind farms and PV systems, are located relatively far from the generators, the impact is expected to be less eminent. In summary, the impact is rather system subjective depending on several factors; hence, a general conclusion cannot be simply drawn. It is necessary to conduct the analysis for any particular system under consideration.

Importantly, it should be cautioned again that losing a large amount of generation can further lead to a significant drop or even collapse of the system frequency. In addition, it is not easy to timely find sufficient generation to make up for the portion removed due to the disconnection of large generating units. To examine this aspect in detail, it requires a time-domain simulation with detailed protection schemes, corrective actions and secondary responses. This is also one of the interesting and challenging topics for the future work.

Chapter 6

Conclusions

This dissertation has examined one of the system operational limits, i.e. transfer capability, which is evaluated through the Total Transfer Capability (TTC) index. As a large penetration of renewable energy is expected within the near future, utilities, universities, and many related entities are now extensively conducting researches, investigations, and experiments just to be prepared for the coming unfamiliar challenges and new problems within. There are several concerns over a large penetration of renewable energy, most of which are related to the system security issues, e.g. the frequency fluctuation, reverse power flow, excess power, system stability, etc. In addition, the uncertainty associated with the renewable energy power output further complicates the system planning and operation more than ever before. The modeling of the renewable energy based generation is therefore important and necessary. The details of the model generally depend on the intended analyses and applications. In addition to the issue related to the renewable energy, system security in terms of voltage and transient stability constraints should also be properly taken into account in the evaluation where a comprehensive scheme is not available at present.

The objective of this research is to develop a comprehensive scheme for the TTC evaluation by means of the probabilistic method taking into account all of the above mentioned issues. Hence, one of the main contributions of this research is to fulfill the need and provide system operators and engineers with a suitable analytical tool. The analytical tool, renewable energy modeling, and research findings presented in this dissertation can be used to attain a more efficient, secure planning and operation of a power system. The developed method employs Monte Carlo simulation which is justified over other probabilistic methods due to its flexibility in handling and incorporating the uncertainty associated with various kinds of parameters ranging from forecast data to equipment availability. The TTC is selected based on the risk concept in which the stochastic nature of a system and fault is fully reflected. Voltage stability is ensured by specifying a sufficient margin away from the voltage collapse point, giving a system a room for unexpected incidences. Transient stability is assessed by the time-domain simulation where the detailed models of a synchronous generator together with its controllers, e.g. an exciter and turbine governor, wind power and PV system can be included.

The developed TTC evaluation scheme is applied to investigate the impact of renewable energy penetration, voltage and transient stability constraints on the TTC. It is found from the investigation that the TTC increases with the increasing renewable energy penetration level, i.e. the system can transfer more power as more renewable energy is installed into the system.

In contrast, the impact of the voltage and transient stabilities is rather system subjective and depends on several factors, e.g. system configuration, generation redispatch, etc. As expected, the TTC decreases due to the voltage and transient stability constraints since some of the transfer has to be reduced.

In addition to the development of the TTC evaluation method, this dissertation further aims at developing a technique to speed up the computation. As is known, the main disadvantage of the Monte Carlo method is its high computation cost as it usually requires a sufficiently large sample size for the convergence of the simulation process. This time-consuming process is the main impediment to its widespread use for the system analysis; hence, the TTC evaluation. Moreover, the addition of voltage and transient stability assessment results in an extensive computation burden since a number of cases have to be checked for the voltage stability margin and the time-domain simulation has to be performed for a number of outage cases. This huge computation burden makes the proposed TTC evaluation scheme not applicable for a real-time application or very short-term planning. To overcome such drawback, this research proposes several techniques to help speed up the computation, i.e. voltage stability index, system case partitioning using two filters and decision tree classification.

Commonly used to estimate the proximity away from the voltage collapse point, a voltage stability index is employed here to screen out the cases within the Monte Carlo sample set likely to have an insufficient voltage stability margin. With a proper selection of a threshold, a significant number of cases to be checked during Monte Carlo simulation are reduced; as a result, the run time is saved.

The run time is further saved by reducing the size of the sample set to be evaluated during Monte Carlo simulation. This is done by system case partitioning. The system case partitioning uses two filters to grasp the risk-related cases from the Monte Carlo sample set. The first filter is based on the performance indices which are used to measure the severity of the system condition and based on which it is ranked. The second filter employs a decision tree with one input attribute to roughly screen out the cases prone to transient instability. The results from the two filters are later used to select the cases for the partitioned set.

Besides, another decision tree with more input attributes is used for fast transient stability prediction. Instead of a time-consuming time-domain simulation, the system stability can be quickly assessed by the decision tree based on the classification patterns it learns from the training data. The validation and performance of the proposed speed improvement techniques have been illustrated and verified through numerical simulation. As expected, the simulation result shows that the run time depends on the number of cases used in the partitioned set. In the simulation example, the run time can be saved as much as 71% of the original total run time while still obtaining an accurate TTC value with the error less than 1%. In addition, the result demonstrates the success of the properly trained decision tree in predicting the transient stability. The run time can be further saved if the simulation tasks are distributed to several PC's. This may be possible to realize the proposed method for a real-time application, e.g. an energy management system.

Finally, the impact of Low Voltage Ride-Through (LVRT) on the transient stability and TTC has been studied. The LVRT is imposed by utilities on a generating unit, e.g. wind power or PV system such that it should remain connected to support the system during normally occurring disturbance. A generating unit which cannot ride through the excursion of the voltage during the fault is disconnected mainly to protect its equipment from possible damages due to a high fault current, especially power electronics (i.e. an inverter of a PV system). Disconnection of a generating unit is found to affect the system stability; however, depending on several factors. Some faults which cause a drastic drop in the voltage and lead to the disconnection of a large generating unit, may have a very severe impact on the system stability and frequency stability as the system needs to find generation to match up the portion lost. This can further lead to a cascading failure phenomenon; hence, an undesirable large-scale power interruption. However, such severe faults may not occur frequently or do not occur at all within the specified lead-time. Therefore, the simulation results show only a small impact on the TTC.

In the future, transfer capability evaluation is still expected to be one of the challenging and important tasks for the system operators as it has always been to maintain the system security and, at the same time, achieve the efficient operation. New problems are also expected as a power system evolves with the introduction of new constraints and emerging advanced technologies, renewable energy and communication technologies. This may be possible to allow new methods which are not available at present to be used for the improvement of the transfer capability evaluation; of course, needed to further research. The author hopes that the proposed method together with the findings presented in this dissertation can serve as a basis and analytical tool for the future research and development. Another interesting topic which was already pointed out is the development of a comprehensive scheme for the time-domain simulation fully taking into account LVRT, making it more practical and enabling new discoveries related to the system stability.

Bibliography

[1] "Transmission transfer capability," NERC, Reference document, May 1995.

[2] Transmission Transfer Capability Task Force, "Available Transfer Capability Definitions and Determination," North American Reliability Council, Princeton, NJ, June 1996.

[3] G.C. Ejebe, J.G. Waight, M. Sanots-Nieto, and W.F. Tinney, "Fast Calculation of Linear Available Transfer Capability," *IEEE Trans. on Power Systems*, vol. 15, no. 3, pp. 1112–1116, Aug. 2000.

[4] S. Grijalva, P.W. Saucer, and J.D. Weber, "Enhancement of Linear ATC Calculations by the Incorporation of Reactive Power Flow," *IEEE Trans. on Power Systems*, vol. 18, no. 2, pp. 1112–1116, May 2003.

[5] Y. Xiao and Y.H. Song, "Available Transfer Capability (ATC) Evaluation by Stochastic Programming," *IEEE Power Eng. Rev.*, vol. 20, no. 9, pp. 50–52, Sep. 2000.

[6] R.F. Chang, C.Y. Tsai, C.L. Su, and C.N. Lu, "Method for Computing Probability Distributions of Available Transfer Capability," *Proc. nst. Elect. Eng., Gen., Transm., Distrib.*, vol. 149, no. 4, pp. 5427–431, Jul. 2002.

[7] Kulyos Audomvongseree and Akihiko Yokoyama, "Consideration of an Appropriate TTC by Probabilistic Approach," *IEEE Trans. on Power Systems*, vol. 19, no. 1, pp. 375–383, Feb. 2004.

[8] Ramezani M., Singh C., and Haghifam M.R., "Role of Clustering in the Probabilistic Evaluation of TTC in Power Systems Including Wind Power Generation," *IEEE Trans. on Power Systems*, vol. 24, no. 2, pp. 849–858, May 2009.

[9] Nattawut Paensuwan, Akihiko Yokoyama, S.C. Verma, and Nakachi Yoshiki, "Investigation of Impact of Renewable Energy Penetration on System Total Transfer Capability at Risk," *IEEJ Trans. on Power and Energy*, vol. 129, no. 12, pp. 1523–1531, Dec. 2009.

[10] Rong-fu Sun, Yue Fan, Yong-hua Song, and Yuan-zhang Sun, "Development and Application of Software for ATC Calculation," *PowerCon 2006, International Conf. on Power Sys. Tech., 2006*, pp. 1–5, Oct. 2006.

[11] Liang Min, and Abur, A., "Total Transfer Capability Computation for Multi-Area Power Systems," *IEEE Trans. on Power Systems*, vol. 21, no. 3, pp. 1141–1147, Aug. 2006.

[12] Ajjarapu, V., and Christy, C., "The continuation power flow: A tool for steady state voltage stability analysis," *IEEE Trans. on Power Systems*, vol. 7, no. 1, Feb. 1992.

[13] Kulyos Audomvongseree and Akihiko Yokoyama, "Application of AC equivalent to total transfer capability evaluation using two-step method," *Proc. PowerCon 2002, Int. Conf. on Power Sys, Tech.*, 2002, vol. 1, pp. 383–387, Oct. 2002.

[14] Yan Ou, and Chanan Singh, "Assessment of Available Transfer Capability and Margins," *IEEE Trans. on Power Systems*, vol. 17, no. 2, MAy 2002.

[15] Kubokawa J., Yue Yuan, Yorino N. Zoka Y., Sasaki H., and Hakim L., "A Solution of Total Transfer Capability Using Transient Stability Constrained Optimal Power Flow," *Proc. PowerTech 2007*, pp. 2018–2022, 2007.

[16] Kumar D.M.V., and Venkaiah C., "Dynamic Available Transfer Capability (DATC) Computation using Intelligent Techniques," *Proc. PowerCon 2008*, pp. 1–6, 2008.

[17] R.A. Rosales, D. Ruiz-Vega, D. Ernst *et al.*, "Online Transient Stability Constrained ATC Calculations," *Proc. IEEE Power Eng. Society Summer Meeting*, pp. 1291–1296, 2000.

[18] Y. Yamada, M. Nagata, and K. Tanaka, "An Energy Function Based on Contingency screening Method for TTC Assessment with Transient Stability Constraints," *Proc. IEEE/PES T&D Conf. and Exhibition*, pp. 886–890, 2002.

[19] Bludszuweit H., Dominguez-Navarro J.A., and Llombart A., "Statistical Analysis of Wind Power Forecast Error," *IEEE Trans. on Power Systems*, vol. 23, no. 3, pp. 983–991, 2009.

[20] Roy Billinton and Wenyuan Li, "Reliability Assessment of Electric Power Systems Using Monte Carlo Methods," New York: Plenum, 1994.

[21] Wenyuan Li, "Risk Assessment of Power Systems," John Wiley & Sons, Inc., 2005.

[22] P. Kundur, "Power system stability and control," McGraw-Hill, Inc., 1994.

[23] Musirin I., Rahman, and T.K.A., "On-Line Voltage Stability Based Contingency Ranking Using Fast Voltage Stability Index (FVSI)," *Proc. Trans. and Dist. Conf. and Exhibition 2002: Asia Pacific. IEEE/PES*, vol. 2, pp. 1118-1123, 2002.

[24] Comparison of High Technical Demands on Grid Connected Wind Turbines Defined in International Grid Codes, EWEC Conf. 2008, Available [online]: http://www.ewec2008proceedings.info/ewec2008/allfiles2/194_EWEC2008fullpaper.pdf.

[25] TRANSPOWER Literature Review Report, "Generator Fault Ride Through Investigation," Feb. 2009.

[26] Available [online]: http://www.meti.go.jp/committe/materials2/downloadfiles/g80908a04j.pdf.

[27] A. E. Feijdoo and J. Cidras, "Modeling of Wind Farms in the Load Flow Analysis," *IEEE Trans. on Power Systems*, vol. 15, no. 1, pp. 110–115, Feb. 2000.

[28] H. Li, Z. Chen, and L. Han, "Comparison and Evaluation of Induction Generator Models in Wind Turbine Systems for Transient Stability of Power System," *Proc. PowerCon 2006*, pp. 1–6, 2006.

[29] Fernandez-Bernal F., Rouco L., Centeno P., Gonzalez M., and Alonso M., "Modeling of Photovoltaic Plants for Power system Dynamic Studies," *Proc. Fifth Int. Conf. on Power Syst. Management and Control*, pp. 341–346, 2002.

[30] Luo X., Patton A.D., and Singh C., "Real Power Transfer Capability Calculations Using Multi-Layer Feed-Forward Neural Networks," *IEEE Trans. on Power Systems*, vol. 15, no. 2, pp. 903–908, 2000.

[31] Jain T., Singh S.N., Srivastava S.C., Gonzalez M., and Alonso M., "A Neural Network Based Method For Fast ATC Estimation in Electricity Markets," *Proc. IEEE Power Eng. Society Summer Meeting*, pp. 1–8, 2007.

[32] Pandey S.N., Pandey N.K., Tapaswi S., and Srivastava L., "Neural Network-Based Approach for ATC Estimation Using Distributed Computing," *IEEE Trans. on Power Systems*, vol. 25, no. 3, pp. 1291–1300, 2010.

[33] Pandey S.N., Pandey N.K., Tapaswi S., and Srivastava L., "Total Transfer Capability Computation for Multi-Area Power Systems," *IEEE Trans. on Power Systems*, vol. 21, no. 3, pp. 1141–1147, 2006.

[34] George K. Stefopoulos, Fang Yang, George J. Cokkinides, and A. P. Sakis Meliopoulos, "Advanced Contingency Selection Methodology," *Proc. 37th Annual North American Power Symp.*, pp. 67–73, 2005.

[35] Hatziargyriou N.D., Contaxis G.C., and Sideris N.C., "A Decision Tree Method for On-Line Steady State Security Assessment," *IEEE Trans. on Power Systems*, vol. 9, no. 2, pp. 1052–1061, May 1994.

[36] Rovnyak S., Kretsinger S., Thorp J., and Brown D., "Decision Trees for Real-Time Transient Stability Prediction," *IEEE Trans. on Power Systems*, vol. 9, no. 3, pp. 1417–1426, Aug. 1994.

[37] Hatziargyriou N.D., Papathanassiou S.A., and Papadopoulos M.P., "Decision Trees for Fast Security Assessment of Autonomous Power Systems with a Large Penetration from Renewables," *IEEE Trans. on Power Systems*, vol. 10, no. 2, pp. 315–325, June 1995.

[38] Kai Sun, Likhate S., Vittal V., Kolluri V.S., and Mandal S., "An Online Dynamic Security Assessment Scheme Using Phasor Mea-surements and Decision Trees," *IEEE Trans. on Power Systems*, vol. 22, no. 4, pp. 1935–1943, Nov. 2007.

[39] Mitchell Tom, Machine Learning, New York: McGraw-Hill, Inc., 1997.

[40] Thomas H. Cormen, Charles E. Leiserson, Ronald L. Rivest, and Clifford Stein, "Introduction to Algorithms," Second Edition, MIT Press and McGraw-Hill, 2001.

[41] L. Goel and R. Billinton, "A Procedure for Evaluating Interrupted Energy Assessment Rates in an Overall Electric Power System," *IEEE Trans. on Power Systems*, vol. 6, pp. 1390–1403, Aug. 1991.

Appendix A

Test System Data

The data of the test systems, modified WSCC 9-bus system, and modified IEEE 30-bus system, wind power generation and PV system are provided in the following sections.

A.1 WSCC 9-Bus System

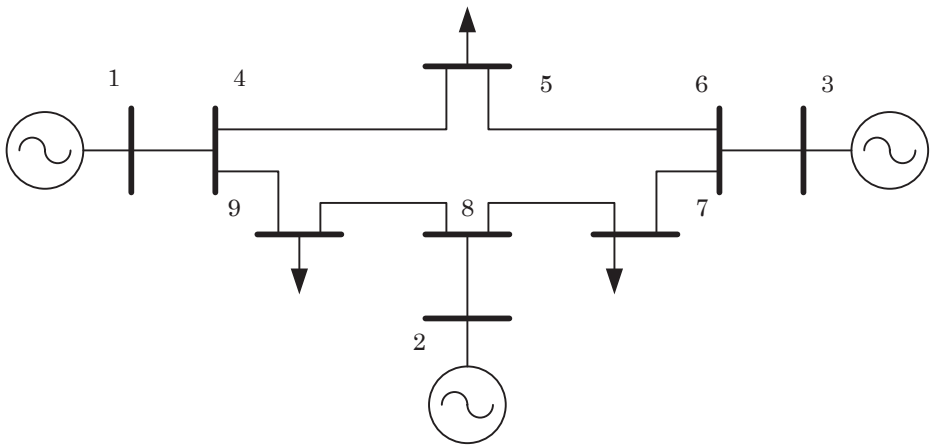

Figure 56: WSCC 9-bus system.

Table 21: Bus data

#	P_D [MW]	Q_D [MVAr]	G_s	B_s
1	-	-	-	-
2	-	-	-	-
3	-	-	-	-
4	-	-	-	-
5	90.00	30.00	-	-
6	-	-	-	-
7	100.00	35.00	-	-
8	-	-	-	-
9	125.00	50.00	-	-

Table 22: Branch data

#	From	To	No. of circuits	Data per circuit			
				R [p.u.]	X [p.u.]	B [p.u.]	Rating [MVA]
1	1	4	2	-	0.1152	-	125
2	4	5	2	0.0340	0.1840	0.0790	125
3	5	6	2	0.0780	0.3400	0.1790	75
4	3	6	2	-	0.1172	-	150
5	6	7	2	0.0238	0.2016	0.1045	75
6	7	8	2	0.0170	0.1440	0.0745	125
7	8	2	2	-	0.1250	-	125
8	8	9	2	0.0640	0.3220	0.1530	125
9	9	4	2	0.2000	0.1700	0.0880	125

Table 23: Generator data

#	Bus#	$P_{\min}$ [MW]	$P_{\max}$ [MW]	$Q_{\min}$ [MVAr]	$Q_{\max}$ [MVAr]
1	1	10.00	250.00	-300.00	300.00
2	2	10.00	300.00	-300.00	300.00
3	3	10.00	270.00	-300.00	300.00

A.2 IEEE 30-Bus System

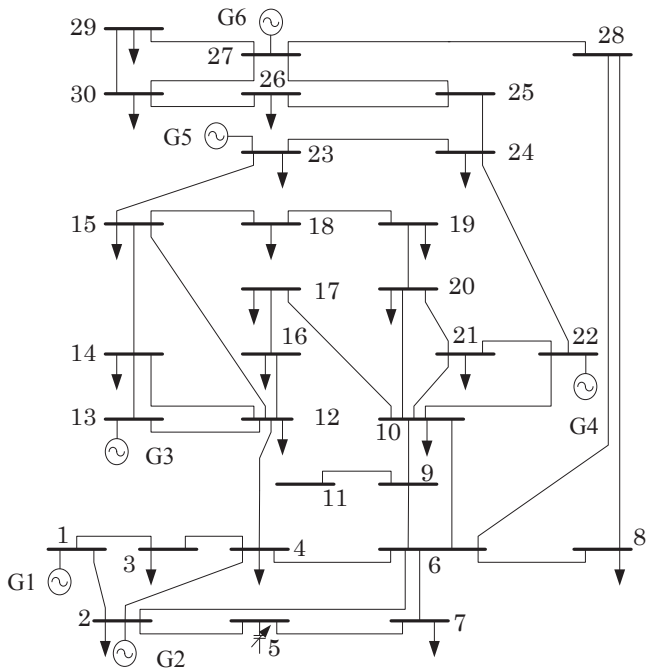

Figure 57: IEEE 30-bus system.

The following data are used for the simulation conducted in Section 5.1.

Table 24: Bus data

#	P_D [MW]	Q_D [MVAr]	G_s	B_s
1	-	-	-	-
2	35.805	13.97	-	-
3	3.96	1.32	-	-
4	12.54	1.76	-	-
5	-	-	-	0.19
6	-	-	-	-
7	37.62	11.99	-	-
8	49.50	33.00	-	-
9	-	-	-	-
10	9.57	2.20	-	-
11	-	-	-	-
12	18.48	8.25	-	-
13	-	-	-	-
14	10.23	1.76	-	-
15	13.53	2.75	-	-
16	5.775	1.98	-	-
17	14.85	6.38	-	-
18	5.28	0.99	-	-
19	15.675	3.74	-	-
20	3.63	0.77	-	-
21	28.875	12.32	-	-
22	-	-	-	-
23	5.28	1.76	-	-
24	14.355	7.37	-	0.04
25	-	-	-	-
26	5.775	2.53	-	-
27	-	-	-	-
28	-	-	-	-
29	3.96	0.99	-	-
30	17.49	2.09	-	-

Table 25: Branch data

#	From	To	No. of circuits	Data per circuit			
				R [p.u.]	X [p.u.]	B [p.u.]	Rating [MVA]
1	1	2	2	0.040	0.120	0.015	260
2	1	3	2	0.040	0.120	0.010	260
3	2	4	1	0.060	0.170	0.020	260
4	3	4	1	0.100	0.040	-	520
5	2	5	2	0.100	0.400	0.010	260
6	2	6	1	0.060	0.180	0.020	260
7	4	6	1	0.010	0.040	-	360
8	5	7	1	0.050	0.120	0.010	280
9	6	7	2	0.060	0.160	0.005	260
10	6	8	2	0.020	0.080	-	128
11	6	9	1	-	0.210	-	260
12	6	10	1	-	0.560	-	128
13	9	11	2	-	0.420	-	128
14	9	10	2	-	0.220	-	128
15	4	12	1	-	0.260	-	260
16	12	13	2	-	0.280	-	128
17	12	14	1	0.120	0.260	-	128
18	12	15	1	0.070	0.130	-	128
19	12	16	1	0.090	0.200	-	128
20	14	15	1	0.220	0.200	-	64
21	16	17	2	0.160	0.380	-	32
22	15	18	1	0.110	0.220	-	64
23	18	19	2	0.120	0.260	-	32
24	19	20	2	0.060	0.140	-	64
25	10	20	1	0.090	0.210	-	128
26	10	17	2	0.060	0.160	-	64
27	10	21	1	0.030	0.070	-	128
28	10	22	1	0.070	0.150	-	128
29	21	22	1	0.010	0.020	-	260
30	15	23	2	0.200	0.400	-	32

Table 26: Branch data (Cont.)

#	From	To	No. of circuits	Data per circuit			
				R [p.u.]	X [p.u.]	B [p.u.]	Rating [MVA]
31	20	21	1	0.120	0.180	-	64
32	22	24	1	0.120	0.180	-	64
33	23	24	1	0.130	0.270	-	64
34	24	25	2	0.380	0.660	-	32
35	25	26	2	0.500	0.760	-	32
36	25	27	1	0.110	0.210	-	64
37	28	27	1	-	0.400	-	260
38	27	29	2	0.440	0.840	-	32
39	27	30	1	0.320	0.600	-	64
40	29	30	1	0.240	0.450	-	64
41	8	28	1	0.060	0.200	0.020	128
42	13	14	1	0.320	0.600	-	64
43	26	30	1	0.320	0.600	-	64

Table 27: Generator data

#	Bus#	$P_{\min}$ [MW]	$P_{\max}$ [MW]	$Q_{\min}$ [MVAr]	$Q_{\max}$ [MVAr]
1	1	0.00	400.00	-100.00	150.00
2	2	0.00	80.00	-100.00	150.00
3	13	0.00	40.00	-100.00	100.00
4	22	0.00	50.00	-100.00	100.00
5	23	0.00	30.00	-100.00	100.00
6	27	0.00	55.00	-100.00	100.00

The following data are used for the simulation conducted in Section 5.2.

Table 28: Bus data

#	P_D [MW]	Q_D [MVAr]	G_s	B_s
1	-	-	-	-
2	23.87	13.97	-	-
3	2.64	1.32	-	-
4	8.36	1.76	-	-
5	-	-	-	0.19
6	-	-	-	-
7	25.08	11.99	-	-
8	33.00	33.00	-	-
9	-	-	-	-
10	6.38	2.20	-	-
11	-	-	-	-
12	12.32	8.25	-	-
13	-	-	-	-
14	6.82	1.76	-	-
15	9.02	2.75	-	-
16	3.85	1.98	-	-
17	9.90	6.38	-	-
18	3.52	0.99	-	-
19	10.45	3.74	-	-
20	2.42	0.77	-	-
21	19.25	12.32	-	-
22	-	-	-	-
23	3.52	1.76	-	-
24	9.57	7.37	-	0.04
25	-	-	-	-
26	3.85	2.53	-	-
27	-	-	-	-
28	-	-	-	-
29	2.64	0.99	-	-
30	11.66	2.09	-	-

Table 29: Branch data

#	From	To	No. of circuits	Data per circuit			
				R [p.u.]	X [p.u.]	B [p.u.]	Rating [MVA]
1	1	2	2	0.040	0.120	0.015	65
2	1	3	2	0.040	0.120	0.010	65
3	2	4	1	0.060	0.170	0.020	65
4	3	4	1	0.100	0.040	-	130
5	2	5	2	0.100	0.400	0.010	65
6	2	6	1	0.060	0.180	0.020	65
7	4	6	1	0.010	0.040	-	90
8	5	7	1	0.050	0.120	0.010	70
9	6	7	2	0.060	0.160	0.005	260
10	6	8	2	0.020	0.080	-	32
11	6	9	1	-	0.210	-	65
12	6	10	1	-	0.560	-	32
13	9	11	2	-	0.420	-	32
14	9	10	2	-	0.220	-	32
15	4	12	1	-	0.260	-	65
16	12	13	2	-	0.280	-	32
17	12	14	1	0.120	0.260	-	32
18	12	15	1	0.070	0.130	-	32
19	12	16	1	0.090	0.200	-	32
20	14	15	1	0.220	0.200	-	16
21	16	17	2	0.160	0.380	-	8
22	15	18	1	0.110	0.220	-	16
23	18	19	2	0.120	0.260	-	8
24	19	20	2	0.060	0.140	-	16
25	10	20	1	0.090	0.210	-	32
26	10	17	2	0.060	0.160	-	16
27	10	21	1	0.030	0.070	-	32
28	10	22	1	0.070	0.150	-	32
29	21	22	1	0.010	0.020	-	65
30	15	23	2	0.200	0.400	-	8

Table 30: Branch data (Cont.)

#	From	To	No. of circuits	Data per circuit			
				R [p.u.]	X [p.u.]	B [p.u.]	Rating [MVA]
31	20	21	1	0.120	0.180	-	16
32	22	24	1	0.120	0.180	-	16
33	23	24	1	0.130	0.270	-	16
34	24	25	2	0.380	0.660	-	8
35	25	26	2	0.500	0.760	-	8
36	25	27	1	0.110	0.210	-	16
37	28	27	1	-	0.400	-	65
38	27	29	2	0.440	0.840	-	8
39	27	30	1	0.320	0.600	-	16
40	29	30	1	0.240	0.450	-	16
41	8	28	1	0.060	0.200	0.020	32
42	13	14	1	0.320	0.600	-	16
43	26	30	1	0.320	0.600	-	16

Table 31: Generator data

#	Bus#	$P_{\min}$ [MW]	$P_{\max}$ [MW]	$Q_{\min}$ [MVAr]	$Q_{\max}$ [MVAr]
1	1	0.00	120.00	-20.00	150.00
2	2	0.00	80.00	-20.00	60.00
3	13	0.00	40.00	-15.00	44.70
4	22	0.00	50.00	-15.00	62.50
5	23	0.00	30.00	-10.00	40.00
6	27	0.00	55.00	-15.00	48.70

A.3 Wind Power Generation and PV System Data

The data of an induction generator of the wind power system and the data of the PV system are given in this section. The parameters are in per unit on machine base. The current limiters of the power regulator of a PV system as shown in Figure 18 are determined from the generation capacity of a PV system. Wind farms and PV systems are connected to the grid via a transformer with the reactance of 0.10 per unit on system base of 100 MVA. The size of the capacitor banks installed at each wind farm is 4 MVAr.

Table 32: Induction generator data

$\mathrm{MVA}_{\mathrm{base}}$	R_s	X_s	X_m	R_r	X_r	H_m	$H_{\omega r}$	K_s
2.25	0.048	0.075	3.8	0.018	0.120	3.0	1.0	0.3

Table 33: PV system data

Active power		Reactive power		T [sec]
K_p	K_i	K_p	K_i	
0.05	0.50	0.05	0.50	0.01

Appendix B

Sequential Quadratic Programming (SQP)

Sequential Quadratic Programming (SQP) is one of the methods suitable to solve constrained non-linear problems. A brief description of the SQP formulation is given in the section.

Given an optimization problem written in a general form as follows:

$$\left.\begin{array}{l} \min \quad f(x) \\ \text{s.t.} \\ G(x) = 0 \\ H(x) \leq 0 \end{array}\right\} \tag{B.1}$$

where x is a vector of control and state variables, $G(x, \lambda)$ are a set of equality constraints, and $H(x, \lambda)$ are a set of inequality constraints.

SQP will reduce the original optimization problem into a quadratic programming sub-problem which is later solved based on Kuhn-Tucker conditions. The procedure of SQP are listed as follows:

1. Formulate Lagrange function.

$$L(x,\, \lambda) = f(x) + \lambda_G G(x) + \lambda_H H(x). \tag{B.2}$$

   Here λ_G, λ_H are the Lagrange multipliers for the equality and inequality constraints respectively.

2. Define the quadratic programming sub-problem.

$$\left.\begin{array}{l} \min \quad \nabla f^T\left(x_k\right) s_k + 0.5 s_k^T H_k s_k \\ \text{s.t.} \\ G\left(x_k\right) + \nabla G^T\left(x_k\right) s_k = 0 \\ H\left(x_k\right) + \nabla H^T\left(x_k\right) s_k \leq 0 \end{array}\right\}. \tag{B.3}$$

   Here k is the iteration number, and H_k is the positive definite Hessian matrix.

3. Set a new point.

$$x_{k+1} = x_k + \alpha_k s_k. \tag{B.4}$$

Here α_k is the optimal step length along the search direction of s_k. The search direction is determined by solving the following merit function

$$\min\left(f\left(x_{k+1}\right)+\lambda_G G\left(x_{k+1}\right)+\lambda_H \max\left\{0, H\left(x_{k+1}\right)\right\}\right). \tag{B.5}$$

4. Stop the iteration if the procedure converges. The Hessian matrix is updated using Quasi-Newton's method.

$$H^{k+1}=H_k-\frac{H_k^T d_k d_k^T H_k}{d_k^T H_k d_k}+\frac{\gamma\gamma^T}{d_k^T d_k} \tag{B.6}$$

$$d_k=x_{k+1}-x_k \tag{B.7}$$

$$\gamma=\theta Q_k+(1-\theta)H_k d_k \tag{B.8}$$

$$Q_k=\nabla_x L\left(x_{k+1},\lambda_{k+1}\right)-\nabla_x L\left(x_k,\lambda_k\right) \tag{B.9}$$

$$\theta=\begin{cases}1.0, & \text{if} \quad d_k^T Q_k \geq 0.2 d_k^T H_k d_k \\ \frac{0.8 d_k^T H_k d_k}{d_k^T H_k d_k-d_k^T Q_k}, & \text{otherwise}\end{cases}. \tag{B.10}$$

The constants 0.2 and 0.8 can be adjusted based on numerical experience.

Appendix C

Dijkstra's Algorithm

Dijkstra's algorithm is a graph search algorithm for the shortest path of a graph with nonnegative weight edges. The term weight in this content can refer to the cost, distance or impedance. This algorithm is widely used in network routing protocols, most notably IS-IS and OSPF.

The algorithm finds the shortest path, i.e. the path with the lowest cost, between a given source vertex and any other vertices in the graph based on greedy search. The algorithm can be summarized as follows:

1. Define a source vertex.
2. Assign the distance of every vertex in the graph. Set it to zero for the source vertex and infinity for the other vertices.
3. Mark all nodes as unvisited. Set the source vertex as current.
4. For a current vertex, consider all its unvisited neighbors and compute the distance from the source vertex. If the shorter path is found than the previously recorded, overwrite the distance.
5. After considering all neighbors of the current vertex, mark it as visited. Note that the visited vertex will not be checked again.
6. Set the unvisited vertex with the shortest distance from the source node as the next current vertex.
7. Continue from step 3 until all vertices are visited.

Once finished, the shortest path from the given source vertex to any other vertices in the graph can be obtained from the final recorded distance.

Appendix D

List of Publications

Some of the results presented in this dissertation have been published in the following publications.

Transaction/Journal Papers

1. Nattawut Paensuwan, Akihiko Yokoyama, S.C. Verma, and Yoshiki Nakachi, "Investigation of Impact of Renewable Energy Penetration on System Total Transfer Capability at Risk," *IEEJ Trans. on Power and Energy*, vol. 129, no. 12, Dec. 2009.

2. Nattawut Paensuwan, Akihiko Yokoyama, S.C. Verma, and Yoshiki Nakachi, "Application of Decision Tree Classification to the Probabilistic TTC Evaluation," *Journal of International Council on Electrical Engineering, JICEE*, (To be published in April 2011).

3. Nattawut Paensuwan, Akihiko Yokoyama, Yoshiki Nakachi, and S.C. Verma, "Improved Risk-Based TTC Evaluation with System Case Partitioning," *Trans. on Electrical Power & Energy Systems*, (Under review).

International Conferences Papers

1. Nattawut Paensuwan and Akihiko Yokoyama, "Risk-Based TTC Calculation of a Power System with Renewable Energy Resources," Power Tech 2009, Bucharest, Romania, July 2009.

2. Nattawut Paensuwan and Akihiko Yokoyama, "Probabilistic TTC of a Power System Integrated with Wind Generation Systems," ICEE 2009, Shenyang, China, July 2009.

3. Nattawut Paensuwan and Akihiko Yokoyama, "Risk-Based Dynamic TTC Calculation in a Deregulated Power System with a Large Penetration of Wind Power Generation," CIGRE/IEEE PES Joint Symposium, Calgary, Canada, July 2009.

4. Nattawut Paensuwan and Akihiko Yokoyama, "Probabilistic TTC Calculation with Decision Tree Classification," ISAP 2009, Curitiba, Brazil, Nov. 2009.

5. Nattawut Paensuwan, Akihiko Yokoyama, S.C. Verma, and Yoshiki Nakachi, "Application of Decision Tree Classification to the Probabilistic TTC Evaluation," ICEE 2010, Busan, Korea, July 2010.

6. Nattawut Paensuwan, Akihiko Yokoyama, S.C. Verma, and Yoshiki Nakachi, "Voltage Stability Constrained Risk-Based TTC Evaluation of a Power System with Large Integration of Renewable Energy," POWERCON 2010, Hangzhou, China, Oct. 2010.

7. Nattawut Paensuwan and Akihiko Yokoyama, "Total Transfer Capability Evaluation of a Power System with Renewable Energy," AsiaPES 2010, Phuket, Thailand, Nov. 2010.

Domestic Conferences Papers

1. Nattawut Paensuwan, Akihiko Yokoyama, S.C. Verma, and Yoshiki Nakachi, "TTC Calculation with Probabilistic Transient Stability Assessment," Joint Technical Meeting on Power Engineering and Power System Engineering, I.E.E. of Japan, Aug. 2008.

2. Nattawut Paensuwan, Akihiko Yokoyama, S.C. Verma, and Yoshiki Nakachi, "Dynamic TTC Calculation in Power System with Wind Power Generations," National Convention Record, I.E.E. of Japan, Mar. 2009.

3. Nattawut Paensuwan, Akihiko Yokoyama, S.C. Verma, and Yoshiki Nakachi, "Investigation of Impact of Renewable Energy Penetration on System Total Transfer Capability at Risk," 20th Annual Conference of Power & Energy Society, I.E.E. of Japan, Aug. 2009.

4. Nattawut Paensuwan, Akihiko Yokoyama, S.C. Verma, and Yoshiki Nakachi, "Application of Decision Tree Classification to Dynamic TTC Calculation," Joint Technical Meeting on Power Engineering and Power System Engineering, I.E.E. of Japan, Sep. 2009.

5. Nattawut Paensuwan, Akihiko Yokoyama, S.C. Verma, and Yoshiki Nakachi, "Application of Voltage Stability Index to the Total Transfer Capability Evaluation," National Convention Record, I.E.E. of Japan, Mar. 2010.

6. Nattawut Paensuwan, Akihiko Yokoyama, S.C. Verma, and Yoshiki Nakachi, "Total Transfer Capability Evaluation of a Power System with Wind Power Generation," 21st Annual Conference of Power & Energy Society, I.E.E. of Japan, Aug. 2010.

7. Nattawut Paensuwan, Akihiko Yokoyama, S.C. Verma, and Yoshiki Nakachi, "Efficient TTC Evaluation Method with System Case Partitioning Method," Joint Technical Meeting on Power Engineering and Power System Engineering, I.E.E. of Japan, Sep. 2010.